Protein arginine methyltransferases interact with intraflagellar transport particles and change location during flagellar growth and resorption

Katsutoshi Mizuno[a,†] and Roger D. Sloboda[a,b,*]
[a]Department of Biological Sciences, Dartmouth College, Hanover, NH 03755; [b]Marine Biological Laboratory, Woods Hole, MA 02543

ABSTRACT **Changes in protein by posttranslational modifications comprise an important mechanism for the control of many cellular processes. Several flagellar proteins are methylated on arginine residues during flagellar resorption; however, the function is not understood. To learn more about the role of protein methylation during flagellar dynamics, we focused on protein arginine methyltransferases (PRMTs) 1, 3, 5, and 10. These PRMTs localize to the tip of flagella and in a punctate pattern along the length, very similar, but not identical, to that of intraflagellar transport (IFT) components. In addition, we found that PRMT 1 and 3 are also highly enriched at the base of the flagella, and the basal localization of these PRMTs changes during flagellar regeneration and resorption. Proteins with methyl arginine residues are also enriched at the tip and base of flagella, and their localization also changes during flagellar assembly and disassembly. PRMTs are lost from the flagella of *fla10-1* cells, which carry a temperature-sensitive mutation in the anterograde motor for IFT. The data define the distribution of specific PRMTs and their target proteins in flagella and demonstrate that PRMTs are cargo for translocation within flagella by the process of IFT.**

Monitoring Editor
Keith G. Kozminski
University of Virginia

Received: Nov 10, 2016
Revised: Mar 3, 2017
Accepted: Mar 8, 2017

INTRODUCTION

Cilia and flagella (here used as interchangeable terms) are well-conserved organelles that project from the cell body and are found on diverse eukaryotic cell types from unicellular protists to human cells. Flagella comprise >600 different polypeptides (Pazour *et al.* 2005), and defects in motile cilia can be the cause of a heterogeneous set of human phenotypes collectively called primary ciliary dyskinesia (Afzelius, 2004; Lee, 2011). Sliding of flagellar doublet microtubules via the dynein arms is indispensable for motility (Summers and Gibbons, 1971), which is controlled by the radial spokes and central pair apparatus (Smith and Yang, 2004). Collectively the outer doublets, central pair apparatus, radial spokes, and dynein arms comprise the axoneme, a protein complex that is held together by noncovalent interactions. In addition to the flagella of sperm and the motile cilia of the airway, fallopian tubes, efferent ducts of the rete testis, and the ependyma of the brain, a single nonmotile cilium lacking the central apparatus, spokes, and arms, called the primary cilium, is also present on almost all mammalian cell types. Defects in primary cilia are associated with many human disorders, collectively referred to as ciliopathies. Some are relatively minor in effect (e.g., polydactyly), whereas others are much more severe (e.g., polycystic kidney disease, Joubert syndrome; Tobin and Beales, 2009).

Assembly, disassembly, and turnover of the axoneme are dependent on a unique motility process called intraflagellar transport (IFT; Kozminski *et al.*, 1993). IFT is a bidirectional transport system; the motor protein kinesin-2 drives the movement of multiprotein complexes called IFT trains toward the flagellar tip (Cole *et al.*, 1998), and cytoplasmic dynein 1b/2 moves IFT trains toward the cell body (Pazour *et al.*, 1999; Porter *et al.*, 1999). Cargo, in the form of axonemal precursors, soluble matrix proteins, and some membrane proteins, is transported to the flagellar tip by anterograde IFT; at the tip, cargo is released, and the trains are remodeled and returned

This article was published online ahead of print in MBoC in Press (http://www.molbiolcell.org/cgi/doi/10.1091/mbc.E16-11-0774) on March 15, 2017.

†Present address: Center for Developmental Biology, RIKEN, 2-2-3 Minatojima-minamimachi, Chuo-ku, Kobe 650-0047 Japan.

*Address correspondence to: Roger D. Sloboda (rds@dartmouth.edu).

Abbreviations used: aDMA, asymmetric dimethyl arginine; HA, hemagglutinin; IBMX, 3-isobutyl-1-methylxanthine; IFT, intraflagellar transport; KAP, kinesin-associated protein; PRMT, protein arginine methyltransferase; sDMA, symmetric dimethyl arginine.

Supplemental Material can be found at:
http://www.molbiolcell.org/content/suppl/2017/03/14/mbc.E16-11-0774v1.DC1

to the cell body carrying cargo generated by turnover at the tip (Lechtreck, 2015). The complete disassembly of a flagellum, which begins at the tip and progresses to the base, is required before mitosis in most cell types in order to release the basal body to participate in mitosis as a centriole in spindle formation (Quarmby and Parker, 2005).

Posttranslational modifications of proteins function in flagellar growth and resorption. For example, phosphorylation plays a key role in both ciliary assembly and disassembly. It has been shown that phosphorylation of the microtubule-depolymerizing kinesin-13 occurs in response to the signal that induces flagellar assembly; the signal to resorb also induces transport of kinesin-13 into the flagellum (Piao *et al.*, 2009). In addition, inhibition of glycogen synthase kinase (GSK3β) by lithium results in longer-than-normal flagella (Nakamura *et al.*, 1987), suggesting that GSK3β plays a role in enforcing flagellar length control. Subsequent work (Wilson and Lefebvre, 2004) showed that tyrosine phosphorylation of flagellar GSK3β increases early in flagellar growth and then decreases as the flagella reach full length. Several other protein kinases, such as Aurora-like kinase (Pan *et al.*, 2004) and NIMA-related kinase (Wloga *et al.*, 2006), are involved in flagellar resorption. The former enzyme activates a pathway required for tubulin deacetylation and hence destabilization (Pugacheva *et al.*, 2007), and the latter pathway activates Kif24, a member of the kinesin-13 family of microtubule-depolymerizing kinesins (Kim *et al.*, 2015). In addition, a CDK-like kinase (FLS1) is required for the disassembly of the distal but not the proximal half of flagella (Hu *et al.*, 2015). Roles for other protein modifications during flagellar generation and resorption have been suggested but not yet clearly elucidated.

In addition to its well-studied nuclear role in histone modification and epigenetic gene regulation, protein methylation also governs protein–protein interactions and cellular signal transduction mechanisms (Biggar and Li, 2015; Liang *et al.*, 2016). Unlike protein phosphorylation, however, the role of cytoplasmic protein methylation is much less well studied (Bedford and Clarke, 2009). Previously we discovered the components of a protein methylation pathway that operates in *Chlamydomonas* flagella and showed that protein methylation on arginine residues is up-regulated during flagellar resorption (Schneider *et al.*, 2008; Sloboda and Howard, 2009; Werner-Peterson and Sloboda, 2013). MetE encodes methionine synthase (the vitamin B12–independent form), and this enzyme is phosphorylated during resorption (Pan *et al.*, 2011). The methionine produced by MetE is then converted into S-adenosyl methionine (SAM), the methyl donor used by most methyltransferases. Protein arginine methyltransferases (PRMTs) catalyze the transfer of the methyl group from SAM to a guanidino-group nitrogen on arginine (McBride and Silver, 2001). Methylation by PRMTs occurs in several different forms, two of which are important here: the first is the addition of two methyl groups to one of the guanidino nitrogens of arginine via type I PRMTs, producing asymmetric dimethyl arginine (aDMA). The second places a single methyl group on each of the two guanidino nitrogens, producing symmetric dimethyl arginine (sDMA), catalyzed by type II PRMTs.

At least seven axonemal proteins become methylated on arginine residues during flagellar disassembly (Werner-Peterson and Sloboda, 2013). Here we focus on the enzyme(s) responsible for these modifications. We show that the *Chlamydomonas* genome encodes at least seven PRMTs, four of which we study in detail here (type I PRMT 1, 3, and 10, and PRMT 5, a type II enzyme). These four enzymes are present in a punctate pattern along the length of the flagella, similar to, but not entirely coincident with, the distribution of IFT particles; the PRMTs are also enriched at the flagellar tip. In addition to tip localization, PRMT 1 and 3 also exhibit very strong localization to the flagellar base in the region of the transition zone, and this basal localization changes during the processes of flagellar resorption and regeneration. Proteins with aDMA modifications were also detected at the base and the tip of flagella, as well as in a punctate pattern of distribution similar to that of the PRMTs. Furthermore, the data show that PRMTs are transported by IFT, during flagellar resorption and that the PRMTs can hop onto and off IFT trains at local stations along the length of the flagellum. Our results strongly indicate that PRMTs and aDMA modifications of axonemal proteins in the flagella play key roles in both the assembly and disassembly processes, and it is possible that the process of IFT requires, or is regulated at least in part by, protein methylation.

RESULTS

The *Chlamydomonas* genome encodes at least seven PRMTs

The mammalian genome encodes 10 PRMTs (Bedford and Clarke 2009), which either have been shown to produce dimethyl arginine (PRMT 1, 3–6, and 8) or are suspected of having this activity based on sequence analysis (PRMT 2, 7, and 9–11). PRMT 5 is a type II enzyme that generates sDMA; the others with demonstrated methylation activity are type I enzymes that produce aDMA. To identify the potential PRMT genes in the *Chlamydomonas* genome, we performed a TBLASTN search of the *Chlamydomonas* database (JGI ver5.5), using as query sequences human PRMT 1–3, CARM1 (PRMT4), and PRMT 6–9. The identified sequences were then aligned with PRMT sequences from human, sea urchin, yeast, *Arabidopsis thaliana*, and rice using ClustalW. Supplemental Figure S1 lists PRMT genes in *Chlamydomonas*.

As previously suggested (Werner-Peterson and Sloboda, 2013), *Chlamydomonas* PRMT 1, 3, and 5 were clearly grouped with orthologous PRMTs from the other organisms. In addition, clear orthologues of *Chlamydomonas* PRMT 4/CARM 1 and PRMT 7 were identified. On the other hand, orthologues of human PRMT 2, 6, 8, and 9 were not identified in the *Chlamydomonas* genome, results consistent with a report (Bachand, 2007) that indicated that PRMT 2, 8, and 9 do not appear to have orthologues in most unicellular eukaryotes. We also note, importantly for the data to follow, that *Chlamydomonas* gene Cre12.g558100, which has been annotated as PRMT 2 (accession number XP_001702822; Merchant *et al.*, 2007), groups with a recently discovered plant type I PRMT gene named PRMT 10 in *Arabidopsis* (Niu *et al.*, 2007) and rice (Ahmad *et al.*, 2011). We will refer to the Cre12.g558100 gene as PRMT 10. Another *Chlamydomonas* gene, Cre01.g051000, has also been annotated as a PRMT (accession number XP_001689769; Merchant *et al.*, 2007); however, this gene did not group with any of the PRMTs from the organisms used in our analysis.

The data that follow address PRMT 1, 3, 5, and 10 in *Chlamydomonas*. We raised peptide antibodies against *Chlamydomonas* PRMT 1 and 10 (Supplemental Figure S2) and identified commercial antibodies that recognize *Chlamydomonas* PRMT 3 and 5 (Supplemental Figure S3). We have not yet obtained or identified reliable antibodies to the remaining *Chlamydomonas* PRMTs.

Localization of PRMTs in flagella

To understand the function of PRMT-mediated protein methylation in flagellar assembly and disassembly, we used antibodies against PRMT 1, 3, 5, and 10 in an immunofluorescence analysis of full-length, resorbing, and regenerating flagella. Like IFT particle staining, the four PRMTs examined stain flagella in a punctate pattern along the flagellar length (see also Supplemental Figure S5). For PRMT 1, 5, and 10, staining was relatively weak, whereas that of

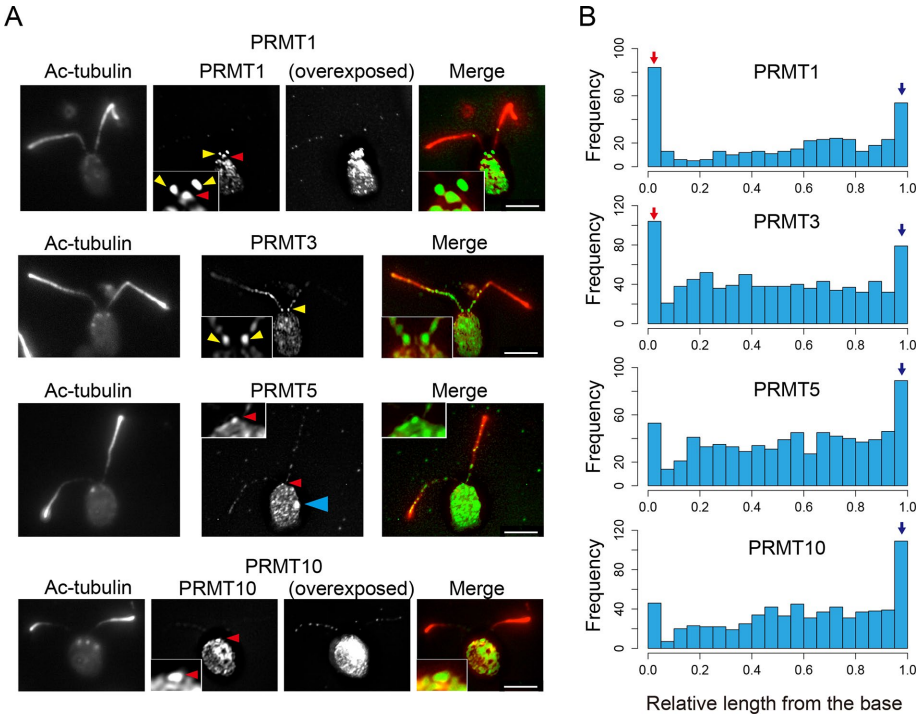

FIGURE 1: PRMTs localize in flagella in a punctate pattern and are enriched at the tip; PRMT 1 and 3 are also enriched at the base of flagella. (A) Immunofluorescence microscopy of WT cells using anti–acetylated tubulin antibody (Ac-tubulin; red) and anti-PRMT antibodies (green). PRMT 1, 3, 5, and 10 are present in puncta along the flagella, and PRMT 1 and 3 show a significant enrichment at the flagella base. Yellow arrowheads indicate PRMTs in the proximal region of the flagella. Red arrowheads indicate the apical region of the cell occupied by the basal body. Note also the localization of PRMT 5 to the eyespot (blue arrowhead). Like PRMT 1 and 3, PRMT 5 and 10 localization also occurs where the flagella meet the cell body, that is, the apical region of the cell occupied by the basal bodies. For PRMT 1 and 10, overexposed images are shown in order to make the punctate pattern readily visible. Insets, enlarged images of the flagella base to demonstrate clearly the enrichment of these enzymes at the base. Scale bars, 5 μm. (B) Histogram of PRMT localization along flagella from base to tip. *X*-axis, relative position of PRMT signals from the base (0) to the tip (1.0; see *Materials and Methods* for an explanation of this measurement]. *Y*-axis, number of puncta at each length position. For all PRMTs, the number of puncta detected at the tip (blue arrow) is greater than at other positions along the length. For PRMT 1 and 3, the frequency of basal puncta is remarkable (red arrow). The number of puncta counted for each histogram: PRMT 1, 401 from 137 flagella; PRMT3; 878 from 123 flagella, PRMT 5; 773 from 177 flagella; and PRMT 10, 702 from 153 flagella.

PRMT 3 was much stronger (Figure 1A). In addition to punctate staining, PRMT 1 and 3 also showed very strong enrichment at the base of full-length flagella (Figure 1, A, yellow arrowheads and insets, and B). By comparison, the localization of PRMT 5 and 10 was greater at the distal region of flagella, and accumulation at the flagella base was less (Figure 1B). In addition, enrichment of PRMTs at the tip was evident when we quantified PRMT positions along the relative length of the flagella (Figure 1B). The relative values for the signal intensity patterns were also different among the PRMTs examined. These results suggest a role for these enzymes in flagellar activities specific to the base and tip. Of interest, PRMT 5 also localized very strongly to the eyespot in the cell body (Figure 1A, blue arrowhead). Whereas methylation (aDMA) of arginine residues by PRMT 1 is important in the control of translation of the light-harvesting proteins (Blifernez *et al.*, 2011), a role for other PRMTs, for example, PRMT 5, which produces sDMA, in the eyespot was not reported. In addition, proteomic analysis showed that several other proteins involved in eyespot development also carry methyl arginine modifications (Eitzinger *et al.*, 2015).

To examine the localization of PRMT 1 and 3 at the flagellar base in more detail, we used a strain in which nephrocystin-4, a protein of the distal component of the transition zone, is tagged with hemagglutinin (HA; *NPHP4-HA* cells, a generous gift of George Witman; Awata *et al.*, 2014). Cells were labeled with anti-HA and anti-PRMT 1 or 3. The basal localization of PRMT 1 is adjacent to but does not overlap with that of NPHP4 (Figure 2A), showing that PRMT 1 accumulates at the base of the axoneme at a position distal to the transition zone location of NPHP4. By comparison, the basal localization of PRMT 3 was almost, but not entirely, coincident with the NPHP4-HA staining, indicating that PRMT 3 is a component of the transition zone (Figure 2B). Furthermore, when flagella are detached from the cell body and probed with anti-PRMT 1 antibodies, a strong signal remains at the base of flagella (Figure 2C). Because NPHP4-HA remains with the cell body after flagella detachment (Awata *et al.*, 2014), this observation confirms that PRMT 1 localizes distal to the transition zone. As expected, we never detected PRMT 3 at the base of detached flagella (unpublished data).

Dynamic changes in the localization of PRMT 1 and 3 during resorption and regeneration

We next studied PRMT localization during flagellar regeneration and resorption. Flagellar regeneration was observed after detachment by pH shock, and resorption was induced with 3-isobutyl-1-methylxanthine (IBMX). In cells that have a basal localization of PRMT 1 at the start of the experiment, this localization was gradually lost during both flagella resorption (Figure 3A) and regeneration (Figure 3B). Note, however, that in cells with this basal localization, it can remain high (compare Figure 3A with Figure 3, C and E). At 0 min (i.e., flagella at full length) the percentage of cells in a population with basal PRMT1 localization is 70%. Thus there is some variation in these data that we are unable to explain. Both the frequency and intensity of the PRMT1 signal at the base returned to the levels before treatment by 120 min (Figure 3, A and B). We also quantified the amount of PRMT 1 localization in resorbing flagella as a function of time in IBMX or during regeneration (Figure 3C) to demonstrate this change more clearly. In resorbing flagella, the basal localization of PRMT 1 was still evident after 30 min of resorption; however, localization at the base was less at 60 min (Figure 3C, left). In regenerating cells, PRMT 1 localization at the flagellar base disappears initially because it is a component of the flagellar base (Figure 2C). In regenerating flagella at 30 min postdeflagellation, PRMT 1 was localized uniformly along the length, with no observable preference for the base or the tip (Figure 3C, right). However, localization of PRMT 1 to the base and tip had clearly recovered after 60 min of regeneration (Figure 3C, right).

To analyze these changes in localization quantitatively, we plotted the intensities and the percentages of PRMT 1 localization at

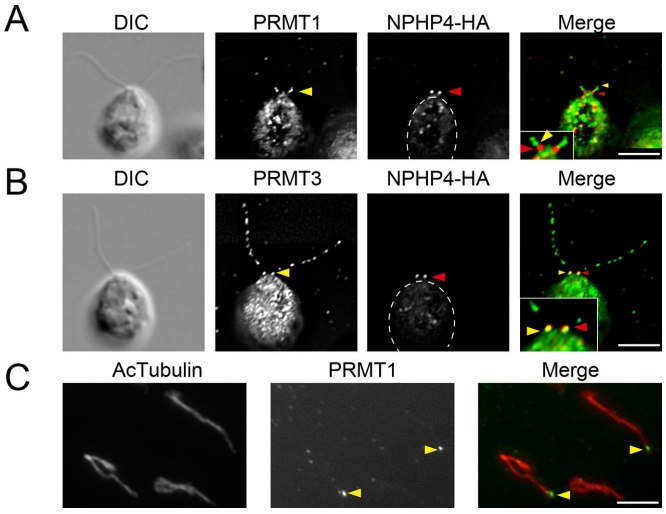

FIGURE 2: PRMT 1 and 3 localization at the base of flagella. (A, B) Immunofluorescence microscopy using cells expressing HA-tagged NPHP4 detected with anti-HA antibody (red). The cells are also labeled (green) with anti-PRMT 1 (A) and anti-PRMT 3 (B). Yellow arrowheads indicate the basal localization of PRMTs. Red arrowheads indicate the location of NPHP-HA. The basal localization of PRMT 1 is more distal than that of NPHP4-HA, a marker of the transition zone. By comparison, a portion of the PRMT 3 signal colocalizes with the NPHP4-HA signal. Insets, expanded images of the flagellar base. (C) Immunofluorescence microscopy of isolated flagella. Flagella are stained with anti–acetylated tubulin (Ac-tubulin; red) and anti-PRMT 1 (green). Localization of PRMT 1 is still detected at the base of the detached flagella, confirming the localization of PRMT 1 at a position distal to the transition zone. Cell bodies are outlined with dashed lines. Scale bars, 5 μm.

the base or the tip as a function of resorption or regeneration time (Figure 3, D and E). In resorbing flagella, the intensities and the percentages of basal localization of PRMT 1 were gradually lost until 45 min of resorption and then recovered (Figure 3, D, left, and E, left, green curves). In cells regenerating their flagella, the localization of PRMT 1 at the base began to recover after 15 min and was similar to the starting distribution by 60 min (Figure 3, D, left, and E, left, red curves). After 45 min of regeneration, flagella with the normal amount of PRMT 1 at the base had begun to recover, and by 90 min, both values were relatively the same as those of full-length flagella (Figure 3E, left, red curve). Overall the decrease and subsequent recovery of PRMT 1 occurred much sooner in regenerating flagella than in resorbing flagella (Figure 3, D, left, and E, left).

In contrast to the basal localization, PRMT 1 enrichment at the flagellar tip responded differently to flagellar dynamics (Figure 3, D and E, right). In regenerating flagella, the signal intensity of PRMT 1 at the flagellar tip increased during regeneration such that at 45 min postdeflagellation, PRMT 1 was enhanced at the tip by a factor of about twofold compared with full-length flagella (Figure 3D, right, red curve). This suggests a role for PRMT 1 in flagellar assembly, which occurs at the distal tip. The initial decrease in the percentage of flagella with tip localization of PRMT 1 observed at early time points (Figure 3E, right, red curve) may be due to our inability to measure accurately very short flagella. In resorbing flagella, both the intensity and percentage of PRMT 1 at the tip gradually decreased until 45 min and then slowly recovered to normal levels (Figure 3, D, right, and E, right, green curves).

The pattern of PRMT 3 localization in flagella was analyzed in a manner similar to that of PRMT 1. PRMT 3 also showed loss of basal localization and recovery of localization at the base after 45 min in both resorbing flagella and regenerating flagella (Figure 4). However, the return of PRMT3 signal at the base occurred more much slowly, if at all; the signal that remained was difficult to detect even after 120 min in both resorbing and regenerating flagella (Figure 4D, left). A decrease in the basal localization percentage of PRMT 3 during 30–45 min was observed both for regenerating and resorbing flagella (Figure 4, D, left, and E, left). In contrast to PRMT1, the intensity of PRMT 3 at the tip was not significantly changed in regenerating flagella (Figure 4D, right, red curve). The percentage of PRMT 3 at the tip was low 15 min after deflagellation but recovered completely by 45 min in regenerating flagella (Figure 4E, right). By comparison, the percentage of PRMT 3 at the tip was not decreased significantly during resorption, and the intensity of PRMT 3 at the tip was weaker than that of PRMT 3 in full-length flagella throughout resorption (Figure 4, D, right, and E, right). Thus changes in localization during flagellar regeneration or resorption differ between PRMT1 and PRMT3, suggesting different roles for these enzymes in flagellar dynamics.

The relative amount of PRMTs in flagella changes during changes in flagellar dynamics

To determine whether the total amount of PRMTs changed in regenerating or resorbing flagella, we analyzed isolated flagella by immunoblotting using antibodies to PRMT 1 and 10 (Figure 5A and Supplemental Figure S2). PRMT 3 and 5 were not studied because available antibodies do not recognize their epitopes in immunoblots. To compare relative PRMT levels, we used flagella from *pf18 fla3*::KAP-GFP cells, in which *fla3* has been transformed with a wild-type (wt) copy of KAP tagged with GFP; FLA3 encodes KAP, the nonmotor subunit of the heterotrimeric IFT motor kinesin-2 (Mueller *et al.*, 2005). The *pf18* mutation causes a loss of the central pair microtubules, and thus the flagella are nonmotile. The amount of IFT88, a component of IFT trains, increased in both resorbing and regenerating flagella compared with full-length, control flagella. By comparison, KAP-GFP greatly increased in regenerating flagella, but the amount in resorbing flagella was not different from controls (Figure 5A).

PRMT 1 appears as a single band and PRMT 10 as a closely spaced doublet on blots (Figure 5A). In resorbing flagella, the amounts of PRMT 1 and PRMT 10 are the same as in full-length flagella. However, in regenerating flagella, a slight shift in the PRMT 1 band to a slower-migrating position and an increase in the amount of the slower-migrating PRMT 10 band of the doublet were observed (Figure 5A). These results suggest that PRMT 1 and PRMT 10 are phosphorylated during the process of flagellar regeneration. Next flagella were fractionated by a freeze–thaw cycle to enrich for flagellar matrix proteins and then extracted with detergent to produce a membrane fraction. In full-length flagella, both PRMT 1 and PRMT 10 were found in the freeze–thaw fraction, indicating that they are either soluble components of the flagellar matrix or only weakly associated with the axoneme. In full-length flagella, PRMT 1 and PRMT 10 were barely detectable in the membrane fraction. On the other hand, there is a significant increase in PRMT 1 and PRMT 10 in the membrane fraction of regenerating flagella (Figure 5B, red boxes). The IFT B complex component IFT88 was present in equal amounts in both the matrix and membrane fractions of full-length and resorbing flagella; however, in regenerating flagella, most of the IFT88 was found in the membrane fraction coincident with a dramatic disappearance of IFT88 from the matrix fraction. Of interest, a significant amount of α-tubulin was also found in the membrane

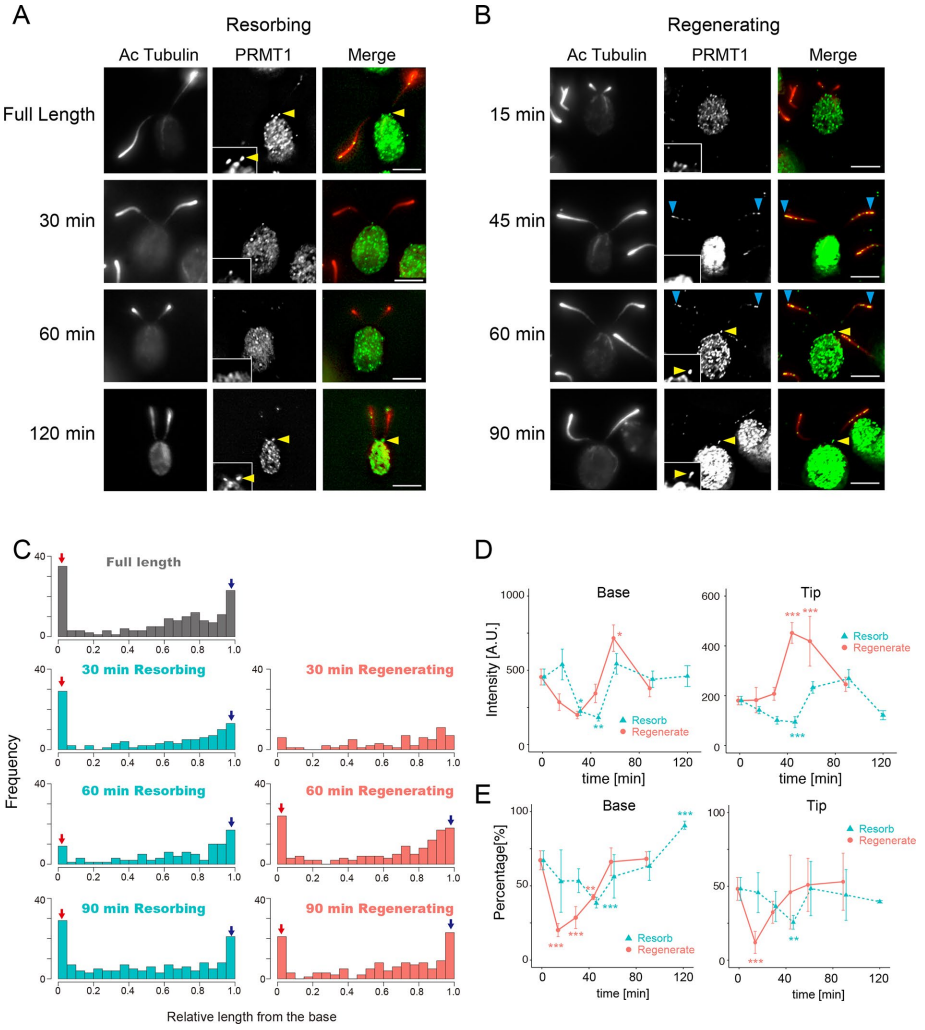

FIGURE 3: PRMT 1 changes localization during flagellar regeneration and resorption. (A) Immunofluorescence microscopy of WT cells with resorbing flagella, using anti–acetylated tubulin (Ac-tubulin, red) and anti-PRMT 1 antibodies (green). PRMT 1 is not often observed at the base of flagella at 30 and 60 min after the initiation of resorption but reappears at the base by 120 min. Insets, enlarged images of the flagellar base. Yellow arrowheads indicate the accumulation of PRMT1 at the proximal end of the flagella. Scale bars, 5 μm. (B) Immunofluorescence microscopy of WT cells with regenerating flagella, using anti–Ac-tubulin (red) and anti-PRMT 1 antibodies (green). PRMT 1 is absent from the base during flagellar regeneration (15–45 min) but reappears at 60–90 min. Insets, enlarged images of the flagellar base. Yellow arrowheads indicate PRMT1 in the proximal end of the flagella. Blue arrowheads indicate localization of PRMT1 at the tip. Scale bars, 5 μm. (C) Histograms of PRMT 1 localization along the length of resorbing (left) and regenerating (right) flagella. Red arrows indicate the relative number of puncta at the base of the flagella, and blue arrows indicate the tip accumulation. (D) Quantification of PRMT 1 intensity at the base (left) and the tip (right) during regeneration (red) or resorption (green). Mean ± SEM from three independent experiments for each time point. For these data, the tip corresponds to the value of 0.95–1.0 in relative flagellar length (the rightmost bin in C). The base corresponds to the value of 0.0–0.05 in relative flagellar length (leftmost bin in C). The number of flagella and puncta analyzed for each time point are listed in Supplemental Table S1. Statistical significance was determined by the Steel–Dwass test. *$p < 0.05$, **$p < 0.01$, ***$p < 0.001$. (E) Comparison of the percentage of flagella with basal PRMT 1 signal (left) and tip PRMT 1 signal (right) during regeneration (red) or resorption (green). Mean ± SEM from three independent experiments. The number of flagella and the number of puncta analyzed are summarized in Supplemental Table S1. Statistical significance was determined by Fisher's exact test, with correction for multiple comparison using Holm's method. *$p < 0.05$, **$p < 0.01$, ***$p < 0.001$.

fraction in regenerating flagella, which likely represents the tubulin being transported to the flagellar tip for use during the flagella regeneration process.

PRMTs and IFT components interact with one another

To determine whether PRMTs interact with IFT particles, immunofluorescence microscopy was performed using flagella from *fla10-1* cells, which carry a temperature-sensitive mutation in the anterograde IFT motor kinesin-2 (Lux and Dutcher, 1991; Piperno and Mead, 1997; Cole *et al.*, 1998). Cells of *fla10-1* were fixed at the permissive (23°C) and restrictive (32°C) temperatures and probed with PRMT and IFT172 antibodies. At the permissive temperature, all PRMTs showed punctate staining along the length of the flagella that was coincident with some, but not all, of the spots identified by IFT172 antibodies (Supplemental Figure S5). PRMT 1 labeling in the mutant flagella was less than in wild-type (WT) cells, and PRMT 1 and 3 showed enrichment at the flagella base (Figure 6, A–E, top), similar to WT cells (Figure 1). By comparison, at the restrictive temperature, both the accumulation at the base and the punctate localization of PRMTs were lost or decreased (Figure 6, A–E, bottom), an observation that was most apparent for PRMT 3 and 5 and less so for PRMT 1 and 10. Quantitative analysis of the labeling showed that the percentage of PRMT 1 and 3 at the base was decreased (Figure 6F, left), and the intensities of PRMT 1 and PRMT 3 at the flagellar base were significantly decreased (Figure 6G, left). By contrast, the percentage of PRMT 1 and PRMT 3 at the flagellar tip was not significantly decreased at the restrictive temperature (Figure 6F, right); however, the intensity of PRMT 3 at the tip was significantly decreased relative to the permissive temperature, although the intensity of PRMT 1 at the tip was not changed (Figure 6G, right). In addition, we compared the signal intensity for all PRMTs along the length of flagella from base to tip. For all PRMTs tested, we observed a significant decrease in signal intensity at the restrictive temperature (Figure 6H). These results strongly suggest that PRMTs are transported by IFT, and IFT is necessary for the maintenance of their normal localization.

Next we fractionated flagella isolated from *fla10-1* cells incubated at the permissive or restrictive temperature and analyzed the results by immunoblotting (Figure 7A). IFT88 was present in normal amounts in flagella at the permissive temperature but was absent from flagella at the restrictive temperature, as expected due to the loss of function of the anterograde IFT motor FLA10 (kinesin-2). Of interest, the relative amounts of PRMT 1 and PRMT 10 in full-length flagella were not affected, even at the restrictive temperature. However, although PRMT 1 and 10 were present

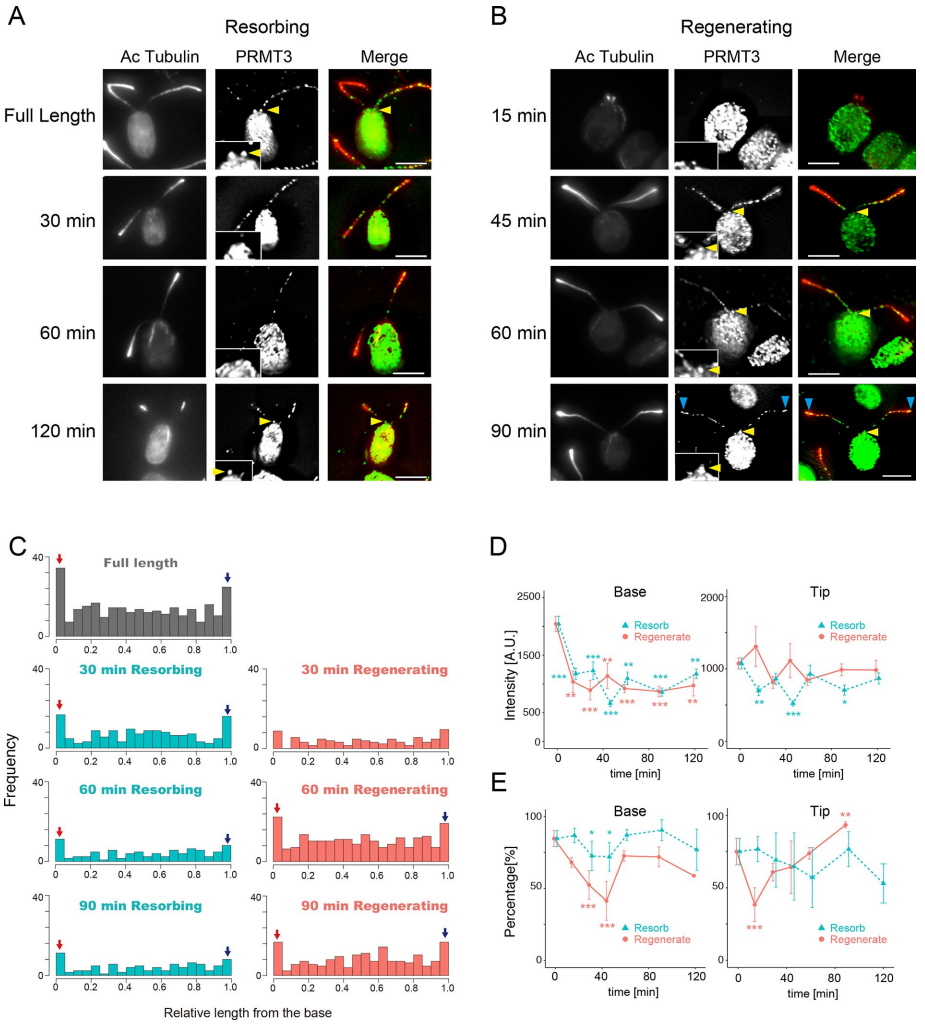

FIGURE 4: PRMT 3 changes localization during flagellar regeneration and resorption. (A) Immunofluorescence microscopy of WT cells with resorbing flagella, using anti–acetylated tubulin (Ac-tubulin, red) and anti-PRMT 3 antibodies (green). PRMT 3 is not detected at the flagellar base during resorption (30–60 min). PRMT 3 reappears at the base by 120 min but with a lower intensity than with full-length flagella. Insets, enlarged images of the flagellar base. Yellow arrowheads indicate the accumulation of PRMT3 at the proximal end of the flagella. Scale bars, 5 µm. (B) Immunofluorescence microscopy of WT cells regenerating flagella, using anti–Ac-tubulin (red) and anti-PRMT 3 antibodies (green). A strong punctate pattern of PRMT 3 along the flagellar length can be detected early in regeneration. PRMT 3 at the base, although present throughout, is weaker during flagellar regeneration than in mature, full-length flagella. Inset, enlarged images of the flagellar base. Yellow arrowheads indicate the PRMT3 in the proximal end of the flagella. Blue arrowheads indicate localization of PRMT3 at the flagellar tip. Scale bars, 5 µm. (C) Red arrows indicate the relative number of puncta at the base of the flagella and blue arrows indicate the tip accumulation. (D) Quantification of PRMT 3 intensity at the base (left) and the tip (right) during regeneration (red) or resorption (green). Mean ± SEM from three independent experiments for each time point. For these data, the tip corresponds to the value of 0.95–1.0 in relative flagellar length (the rightmost bin in C). The base corresponds to the value of 0.0–0.05 in relative flagellar length (leftmost bin in C). The number of flagella and puncta counted for each time point are listed in Supplemental Table S1. Statistical significance was determined by the Steel–Dwass test. *$p < 0.05$, **$p < 0.01$, ***$p < 0.001$. (E) Comparison of the percentage of flagella with basal PRMT 3 signal (left) and tip PRMT 3 signal (right) during flagellar regeneration (red) or resorption (blue). Mean ± SEM from three independent experiments. The numbers of flagella and the number of puncta analyzed are summarized in Supplemental Table S1. Statistical significance was determined by the Fisher's exact test, with correction for multiple comparison using Holm's method. *$p < 0.05$, **$p < 0.01$, ***$p < 0.001$. Scale bar, 5 µm.

in the membrane fraction (NP-40) at 23°C, they were absent from this fraction at 32°C (Figure 7A, red boxes), but the amount of these PRMTs in the matrix fraction (FThaw) was not affected by temperature (Figure 7A). These results suggest that the interaction of PRMT 1 and 10 with IFT components requires the activity of kinesin-2, the motor for anterograde IFT (Figure 5B).

PRMT 1 and 10 interact with IFT particles in resorbing flagella

To test further the interaction between PRMTs and IFT particles and other IFT-related proteins, we performed immunoprecipitation (IP) with extracts from full-length or resorbing flagella from *fla3pf18*::KAP-GFP cells. When we used anti-PRMT 1 for IP, neither IFT139 (an IFT complex A particle component) nor IFT172 (IFT complex B) was precipitated. However, a very small amount of IFT81 was precipitated only from resorbing flagella (Figure 7B, red box). When anti-PRMT 10 was used for IP, KAP-GFP, IFT172, IFT88, IFT81, and IFT139 were precipitated only from resorbing flagella and not from full-length flagella (Figure 7C). These results indicate an interaction of IFT components, and PRMT 1 and 10—in particular PRMT 10—are greatly enhanced in resorbing flagella. We have been unable to immunoprecipitate PRMTs from regenerating flagella.

Localization of flagellar proteins modified with aDMA

To analyze aDMA-modified proteins in flagella, we probed *Chlamydomonas* cells with Asym24 antibodies, which recognize aDMA residues. Immunofluorescence microscopy showed that flagellar proteins with aDMA residues were distributed similarly to PRMT 1 and 3 in flagella. The data revealed a very strong enrichment of dimethylated proteins at the base and tip of the flagella and a punctate distribution along the flagellar length (Figure 8, A and B). The localization of dimethylated proteins at the base was compared with the TZ component of *NPH4-HA* cells; proteins with aDMA modifications are localized both distal to the TZ and at the TZ (Figure 8C), similar to the localization of PRMT 1 and 3 (Figure 2). We quantified the intensity and localization of the Asym24 antibody signal along the length of flagella, and the results demonstrate that proteins modified with aDMA are enriched at the flagellar base and tip in cells with full-length flagella (Figure 8D, top). In regenerating flagella (45 min after deflagellation), there is no accumulation of aDMA-modified proteins detectable at the base; however, there is enrichment at the flagellar tip (Figure 8D, middle). In resorbing flagella (60 min after induction of resorption), enrichment at the base and the tip was similar to that for full-length flagella (Figure 8D, bottom).

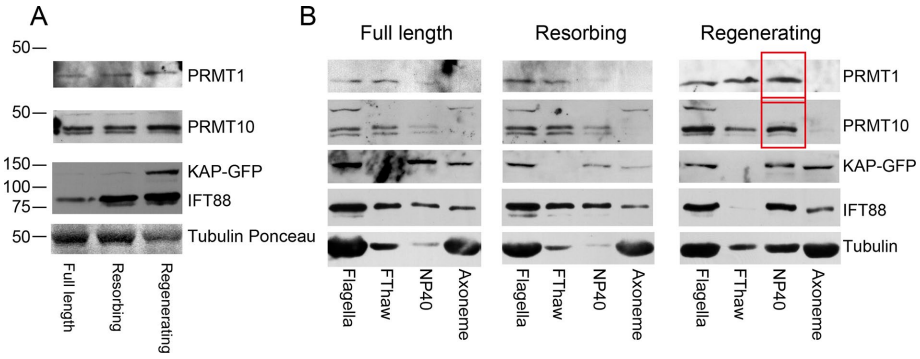

FIGURE 5: PRMT 1 and 10 are enhanced in regenerating and resorbing flagella. (A) Immunoblots of full-length, resorbing, and regenerating flagella using the antibodies indicated. The concentration of each sample was adjusted to 1 mg/ml, and equal volumes of sample were loaded. Tubulin stained with Ponceau S is shown as a loading control. The PRMT 1 band migrates more slowly in samples of regenerating flagella. PRMT 10 always appears as a doublet, and the upper band becomes more pronounced relative to the lower band in regenerating flagella. The amount of IFT88 is greatly increased in both resorbing and regenerating flagella, whereas the amount of KAP-GFP was only observed to increase in regenerating flagella. This is likely because the KAP-GFP lane has been underexposed so as not to overexpose the signal from IFT88. (B) Samples of full-length, resorbing, and regenerating flagella were fractionated into the freeze-thaw supernatant (FThaw), NP-40 extract (membrane fraction), and axonemes, adjusted to 1 mg/ml, separated by SDS–PAGE, and blotted, and the blot was probed with the indicated antibodies. Changes in band intensities as noted in *Results* are indicated with red boxes.

In addition, the intensities of the label at the flagellar base were compared (Figure 8E). In regenerating flagella, the basal intensity of Asym24 staining was not changed until 45 min and then abruptly increased (Figure 8E, left). In addition, the percentage of basal Asym24 signal was significantly decreased during 15–45 min of regeneration time and increased after 60 min (Figure 8E, left). In resorbing flagella, the basal intensity of Asym24 labeling increased, peaked at 45 min of resorption, and subsequently returned to the starting intensity as shortening of the flagella ceased (Figure 8F, left). The percentage of the basal localization of Asym24 in resorbing flagella did not show a large change, although we did detect a slight, significant increase at 30 min (Figure 8F, left).

We also compared the intensities (Figure 8E, right) and percentages (Figure 8F, right) of Asym24 labeling at the flagellar tip. In regenerating flagella, tip intensities gradually increased during the time assayed (90 min); however, the percentage of flagella with tip signal significantly decreased after 15 min of regeneration but recovered to pre-deflagellation levels during the next 15 min of regeneration (Figure 8F, right). In resorbing flagella, tip intensities increased slightly from 30 to 90 min of resorption (Figure 8E, right). The percentage of flagella with Asym24 labeling at the flagellar tip was very high throughout the resorption process, with almost all flagella showing labeling at the tip during resorption (Figure 8F, right). This observation is consistent with a previous report that documented aDMA modification during flagellar resorption (Schneider *et al.*, 2008).

We also compared the signal intensities of Asym24 label along the length of flagella (Supplemental Figure S6). These intensities (in the region of 0.1–0.9 in relative length; see *Materials and Methods*) did not change significantly in regenerating flagella but did significantly increase in resorbing flagella (Supplemental Figure S6, A and B). Combined with previous work (Schneider *et al.*, 2008), these results indicate that proteins with aDMA modifications are produced by the action of PRMTs throughout the flagella. The increase in label noted here could be due to an increase in the labeling and subsequent association of aDMA-modified proteins with IFT trains, an increase in aDMA modifications of IFT complex A or B proteins during flagellar resorption, or both, although we have not yet directly identified any IFT particle proteins that carry methyl modifications.

aDMA modifications show two distinct labeling patterns in the cell body

Asym24 antibodies also labeled the cell bodies in two distinct patterns: 1) weak cell body staining with a strong accumulation of label at the flagellar base, and 2) strong cell body staining that also prevented a clear analysis of the flagellar base (Figure 8, A and B). We also observed labeling at the flagellar tip in cells exhibiting both patterns of cell body staining (Figure 8, A and B, arrowheads). In cells with full-length flagella, the ratio of the two classes of cell body staining was almost 1:1 (Figure 9A, left), but this ratio changed during the processes of flagellar regeneration and resorption. After 45 min of flagellar regeneration, almost all cells observed showed strong cell body staining with Asym24 antibodies (Figure 9A, middle). By contrast, after 60 min of flagellar resorption, almost all cells showed the weak class of cell body staining (Figure 9A, right).

We then compared the intensity of the cell body signal as a function of time in regenerating or resorbing conditions (Figure 9B). In cells with full-length flagella, most of the Asym24 signals had intensity values <~300 (Figure 9B, 0 min) and about half of the cells showed strong cell intensity with varied values. In cells with resorbing flagella, the intensities of cells with the stronger signal were slightly increased, but many cells showed weaker signal intensities (Figure 9B, left). Contrary to this, during flagellar regeneration, most cells showed an increase of labeling intensity by Asym24 antibodies (Figure 9B, right). The percentages of cells with the strong signal were compared during flagellar regeneration and resorption (Figure 9C). The result for flagellar resorption was relatively varied, but in all experiments (Figure 9C, left), there was a slight decrease at first in the percentage of cells with strong label intensity in the cell bodies (around 20–30 min) and a subsequent increase around 45–75 min. Finally, the percentage of cells with strong cell body staining decreased to almost 0% around 80–120 min in all experiments (Figure 9C, left). In cells with regenerating flagella, the response was relatively similar. The percentage of cells with strong cell body signal increased at first (15–30 min) and then showed a subsequent decrease at 45 min of regeneration. After regeneration was complete, the percentage of cells with strong staining in the cell body became close to 50% again (Figure 9C, right). These changes presumably reflect variations in the cytoplasmic activity of PRMT 1, the major type I methyltransferase in cells, in response to flagellar dynamics. Note (Figure 3, A and B) that PRMT1 often localized in the cell body in large spots of uniform diameter, and the intensity of label varied from sample to sample, although we did not quantify this observation.

DISCUSSION

This study demonstrated the following. 1) We identified seven PRMTs in *Chlamydomonas*, four of which (PRMT 1, 3, 5, and 10) localize as punctate spots along the length of the flagella, as well as

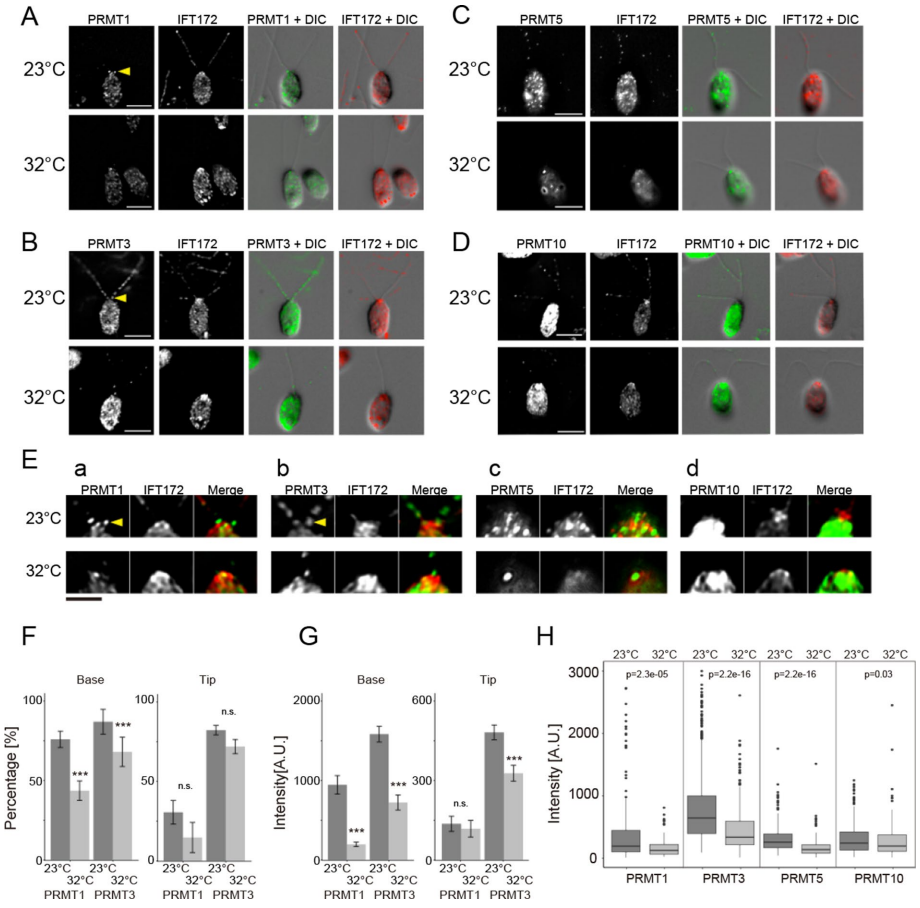

FIGURE 6: PRMT levels are decreased or lost in flagella of *fla10-1* cells shifted to the restrictive temperature. (A–D) Immunofluorescence microscopy of *fla10-1* at the permissive (23°C) and restrictive (32°C) temperatures. Cells were probed with anti-IFT172 (red) and anti-PRMT 1 (A), anti-PRMT 3 (B), anti-PRMT 5 (C), and anti-PRMT 10 (D) (green). The basal, tip, and punctate localizations of the PRMTs noted at the permissive temperature are all weakened or lost at the restrictive temperature. Scale bar, 5 µm. (E) Expanded images of the flagellar bases from A–D. Scale bar, 2.5 µm. Yellow arrowheads in A and B indicate the accumulation of PRMTs in the proximal region of the flagella. (F) Comparison of the percentage of *fla10-1* flagella with basal and tip localizations of PRMT 1 and 3. The percentage of flagella with enhanced PRMT 1 basal localization was significantly decreased at the restrictive temperature; the data for tip localization were not significantly different. Mean ± SEM from three independent experiments. The numbers of flagella and puncta counted along the flagella length are shown in Supplemental Table S2. Statistical significance was determined by the Fisher's exact test, with correction for multiple comparison using Holm's method. ***$p < 0.001$. (G) Comparison of the mean intensity of PRMT 1 and 3 puncta at the flagellar base and tip. Both PRMT 1 and 3 showed a significant decrease in basal intensity at the restrictive temperature. The decrease in tip intensity was significant in PRMT 3 but not in PRMT 1. Mean ± SEM from three independent experiments. The numbers of puncta and flagella counted are shown in Supplemental Table S2. Statistical significance was determined by the Mann–Whitney *U* test. ***$p < 0.001$. (H) Comparison of PRMT spot intensities from the base to the tip of flagella for each of PRMT 1, 3, 5, and 10. All PRMTs showed a significant decrease in intensity at the restrictive temperature. Data from three independent experiments. Numbers of puncta and flagella analyzed are shown in Supplemental Table S2. Statistical significance was determined by the Mann–Whitney U test. *p* values are shown above the data pairs.

at the flagellar tip. 2) PRMT 1 and 3 also localize to distinct regions at the flagellar base, in the area of the transition zone. 3) PRMT localization at the base changes during flagellar regeneration and resorption. 4) PRMT 10 (and perhaps PRMT 1) interacts with IFT particles. 5) IFT is necessary to maintain the normal localization of PRMTs in flagella. 6) Flagellar proteins are modified by methylation at arginine residues, and methylated proteins are found mainly at the flagellar base and tip. 7) Finally, the amount of protein methylation in flagella, as well as in the cell body, changes during flagellar regeneration and resorption.

Phylogenetic analysis of *Chlamydomonas* PRMTs

We identified seven PRMTs (Supplemental Figure S1) encoded in the *Chlamydomonas reinhardtii* genome (JGI ver5.5), as compared with mammals, in which 10 PRMTs have been identified (Bedford, 2007; Bedford and Clarke, 2009; Wei *et al.*, 2014). Most of the focus has been on the role of PRMTs and protein methylation in chromatin organization and gene expression (Jahan and Davie, 2015). The importance of PRMT activity and protein methylation in green algae and plants has recently been gaining attention (Niu *et al.*, 2007; Ahmad *et al.*, 2011; Blifernez *et al.*, 2011), as has PRMT activity outside the nucleus (Herrmann and Fackelmayer, 2009) and in organelles such as the eyespot (Eitzinger *et al.*, 2015) and flagella (Schneider *et al.*, 2008; Sloboda and Howard, 2009; Werner-Peterson and Sloboda, 2013). PRMT 1, 3, and 5 are present in many organisms, from unicellular eukaryotes to mammals (Bachand, 2007). In addition to the 10 mammalian enzymes, there are nine in *Drosophila* and *Arabidopsis* and eight in rice (Ahmad *et al.*, 2011). We searched the *Chlamydomonas* genome for the complement of PRMTs encoded and identified orthologues of mammalian PRMT 1–5 and 7 but not PRMT 6, 8, and 9. PRMT 2 was previously reported to be absent from protists, as are PRMT 8 and 9 (Bachand, 2007). Of interest, we discovered that PRMT 10, a type I PRMT specific to green algae and plants (Niu *et al.*, 2007; Ahmad *et al.*, 2011), has been incorrectly annotated as PRMT 2 in several databases (e.g., Phytozome). A PRMT 10 mutant in *Arabidopsis* (*atPRMT 10-1*) is defective in flowering time (Niu *et al.*, 2007). The seventh PRMT we identified (Cre01.g05100) did not group with any of the known PRMTs examined. Cre01.g05100 is annotated as PRMT 3 at Phytozome, but based on our analysis, this does not appear to be correct either. Perhaps the varying nature of the PRMT genes encoded has arisen because several PRMTs evolved specific to the lineage of bikonts compared with the lineage of the opisthokonts.

PRMTs are transported by IFT

Previously we reported the presence of PRMT 1 in flagella (Werner-Peterson and Sloboda, 2013), and here we showed that additional methytransferases (PRMT 3, 5, and 10) are present as well. PRMT 5 produces sDMA modifications, and the enzyme is present in puncta along the flagella and at the base (Figure 1A). The localization of PRMT 1 and 3 varies with changes in flagellar length. In full-length

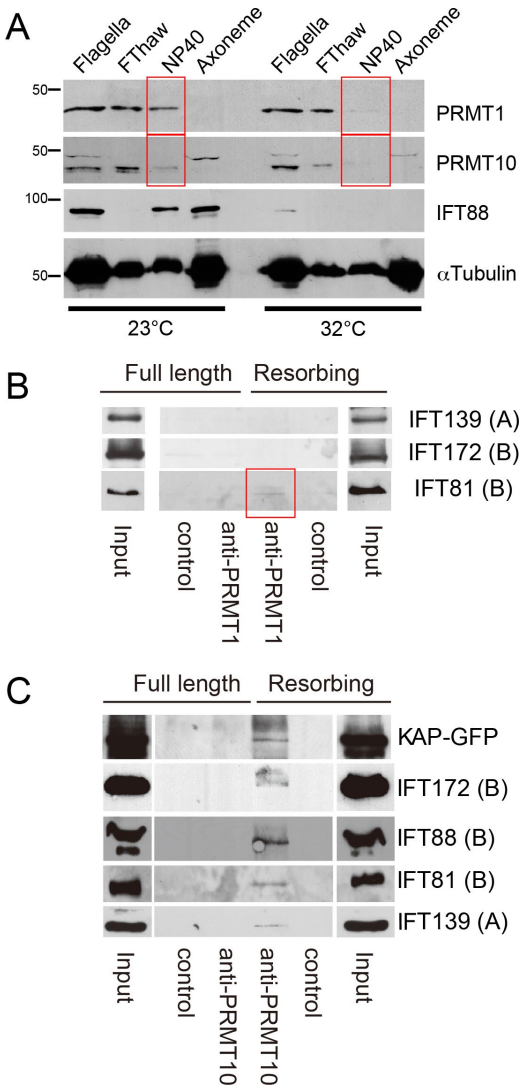

FIGURE 7: PRMT levels in flagella from *fla10-1* cells at the permissive and restrictive temperatures. (A) Immunoblots of flagella from *fla10-1* cells at the permissive and restrictive temperatures. Flagella were fractionated into freeze-thaw supernatant (FThaw), NP-40 extract, and axonemes. The concentration of each sample was adjusted to 1 mg/ml, and equal volumes of sample were separated by SDS–PAGE and probed with the indicated antibodies. Although the relative amounts of PRMT 1 and 10 in intact flagella did not change at the restrictive temperature, PRMT 1 and 10 were absent from the NP-40 extract at the restrictive temperature (red boxes). (B) Immunoblots of an IP experiment using PRMT 1 antibodies. The starting material for IP was an NP-40 extract (membrane plus matrix fraction) of full-length or resorbing flagella isolated from *pf18fla3*::KAP-GFP cells. The input and eluate of each IP was probed with the indicated antibodies. Components of IFT complex A are indicated as (A), and components of IFT complex B are indicated as (B). A small amount of IFT81 was precipitated only from resorbing flagella (red box). (C) Immunoblots of samples immunoprecipitated using PRMT 10 antibodies. The starting material was NP-40 extracts (membrane plus matrix fraction) of full-length and resorbing flagella isolated from *pf18fla3*::KAP-GFP. Both components of IFT complexes A and B, as well as KAP-GFP, were precipitated only from resorbing flagella. Scale bar, 5 μm.

flagella, PRMT 1 and 3 are distributed in a punctate pattern along the flagella, similar to, but not entirely coincident with, the distribution of IFT particles (Figures 1A, and 6, A and B). Accumulation at the flagellar base and the punctate pattern of localization of these PRMTs are similar to those of IFT proteins (Deane *et al.*, 2001). In fact, immunofluorescence microscopy with the *fla10-1* strain (a temperature-sensitive mutant in the IFT motor kinesin-2) showed that localization of PRMTs as punctate spots or accumulation at the tip and base are decreased or lost in cells grown at the restrictive temperature (Figure 6). The association of PRMT 1 and 10 with the membrane fraction is also lost at the restrictive temperature, whereas PRMT 1 and 10 levels in the matrix fraction did not change (Figure 7A). Thus it appears that PRMT 1 and 10 interact with and are likely moved by IFT components, and this interaction is lost when IFT is inhibited. In support of this conclusion is the observation that the amount of PRMT 1 and 10 in the membrane fraction increases in regenerating flagella (Figure 5B), as does the number of IFT particles (Dentler, 2005). Note also that MetE, which produces methionine, is also lost in *fla10* cells at the restrictive temperature (Schneider *et al.*, 2008), raising the possibility that a protein complex (analogous to the methylosome; Friesen *et al.*, 2001) is cargo for IFT.

Immunofluorescence microscopy using Asym24 antibodies showed that flagella have a punctate pattern of aDMA staining (Schneider *et al.*, 2008), as well as enrichment of aDMA residues at the tip and the base of the flagella (Figure 8, A and B). This pattern is similar to but not completely coincident with that of IFT particles, and the intensity of labeling was significantly increased during flagellar resorption (Supplemental Figure S6B). It has been reported that during resorption, several proteins comprising structural elements of the axoneme (radial spoke proteins, tektin, and the nexin-dynein regulatory complex) become modified with aDMA (Werner-Peterson and Sloboda, 2013). These results suggest that the punctate aDMA spots may represent association of one or more of these disassembled axonemal components with the IFT machinery for return to the cell body.

We also observed, via immunoprecipitation, an interaction of PRMT 1 and 10 with IFT components in resorbing flagella (Figure 7, B and C), and this interaction may be mediated by phosphorylation. Mobility shifts in PRMT 1 and 10 suggest that these proteins are phosphorylated during flagellar resorption and regeneration (Figure 5A; Werner-Peterson and Sloboda, 2013). It is possible that phosphorylation of PRMTs regulates the activity of these enzymes or their association with IFT components, a conclusion supported by the following observation: first, protein phosphorylation plays a key role in the resorption process (Pan *et al.*, 2004, 2011; Pugacheva *et al.*, 2007). Indeed, IBMX induces resorption by inhibiting cAMP phosphodiesterase, potentiating the level of cAMP and thus the activity of protein kinase A. Second, the enzyme MetE, which produces methionine from homocysteine, is a flagellar component (Schneider *et al.*, 2008). Methionine is converted into S-adenosyl methionine, the methyl donor in protein methylation reactions. MetE is phosphorylated in resorbing flagella (Schneider *et al.*, 2008; Pan *et al.*, 2011; Plotnikova *et al.*, 2012). Thus the signal to resorb flagella most likely functions via a phosphorylation cascade, and the phosphorylated targets induce tubulin deacetylation (Pugacheva *et al.*, 2007), up-regulation of MetE, and initiation of a downstream protein methylation pathway.

PRMT 1 and 3 are enriched at the flagellar base in addition to being present along the length of the flagella

Of the four PRMTs studied, only PRMT 1 and 3 are enriched at specific positions at the flagellar base (Figure 1, A and B), as are proteins with aDMA modifications (Figure 8C). PRMT 1 localizes just distal to the transition zone (TZ), whereas PRMT 3 localizes at the distal end of the TZ. Together with a complex of transition

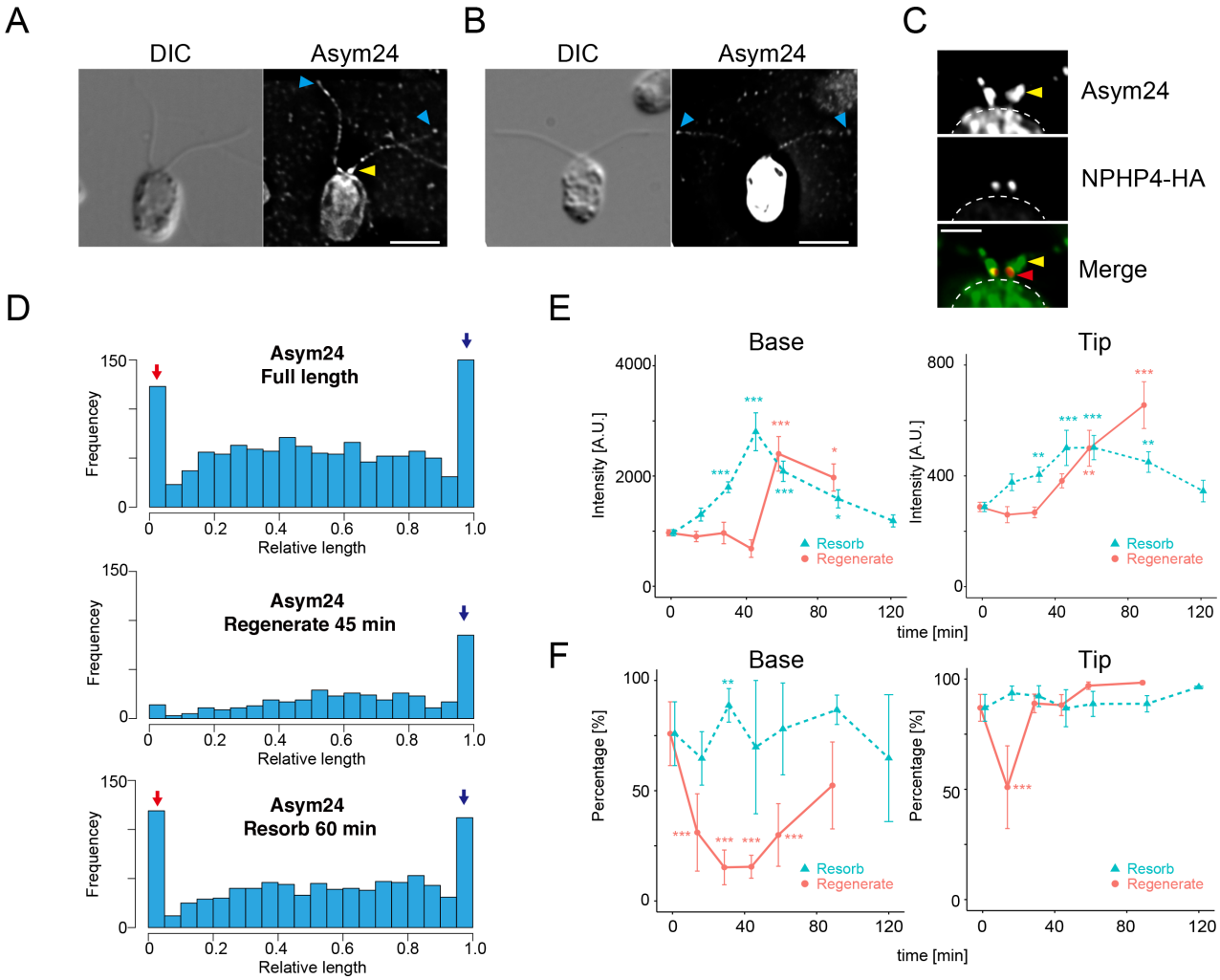

FIGURE 8: Flagellar proteins modified with aDMA are present at the flagellar base and tip. (A) Immunofluorescence microscopy of a WT cell using Asym24 antibodies that label aDMA-modified proteins. In this image, the cell body is not strongly stained. The flagellar base and tip are labeled with Asym24, and a punctate pattern of stain is observed along the flagella length. (B) In comparison to the cell in A, some cells in the same preparation showed very strong labeling of the cell body. Label at the flagellar tip was also observed, but the enrichment at the flagellar base is not clearly visible in cells with strong cell body staining. Yellow arrowheads indicate accumulation of aDMA in the proximal region of the flagella. Blue arrowheads indicate localization of aDMA at the flagellar tip. Scale bar, 5 μm (A, B). (C) Immunofluorescence microscopy of a *NPHP4-HA* cell using Asym24 and anti-HA antibodies. The signal from Asym24 at the flagellar base was observed at the transition zone and at more distal region near the flagellar base. These images are comparable to that of PRMT 1 and PRMT 3 localization (Figure 2). The border of the cell body is indicated by the dashed line. Yellow arrowheads indicate accumulation of aDMA in the proximal region of the flagella. Red arrowheads indicate the location of NPHP-HA. Scale bar, 2 μm. (D) Histograms of Asym24 signal localization along the flagella in cells with full-length flagella (top), regenerating flagella (45 min regenerating; middle), and resorbing flagella (60 min resorbing; bottom). In cells with full-length flagella, the accumulation of Asym24 signal at the flagellar base (red arrow) and the tip (blue arrow) is clearly visible (top). The basal signal of Asym24 is lost in regenerating flagella. but enrichment at the tip is maintained (blue arrow; middle). In resorbing flagella, strong enrichment at the base and the tip is observed (red and blue arrow, bottom). (E) Comparison of Asym24 intensity during flagellar regeneration (red) or resorption (green). Intensity of the flagellar base (left) or tip (right) is plotted as a function of time after the initiation of flagellar resorption or regeneration. Mean ± SEM from three independent experiments. For these data, the tip corresponds to the value of 0.95–1.0 in relative flagellar length (the rightmost bin in D). The base corresponds to the value of 0.0–0.05 in relative flagellar length (leftmost bin in D). Numbers of flagella and puncta for each time point are summarized in Supplemental Table S3. Statistical significance was determined by the Steel–Dwass test. *$p < 0.05$, **$p < 0.01$, ***$p < 0.001$. (F) Comparison of the percentages of flagella with a basal (left) and tip (right) Asym24 signal plotted as a function of the time after initiation of resorption or regeneration. Mean ± SEM from three independent experiments. The number of flagella and puncta counted are summarized in Supplemental Table S3. Statistical significance is determined by the Fisher's exact test, with correction for multiple comparison with Holm's method (**$p < 0.01$, ***$p < 0.001$).

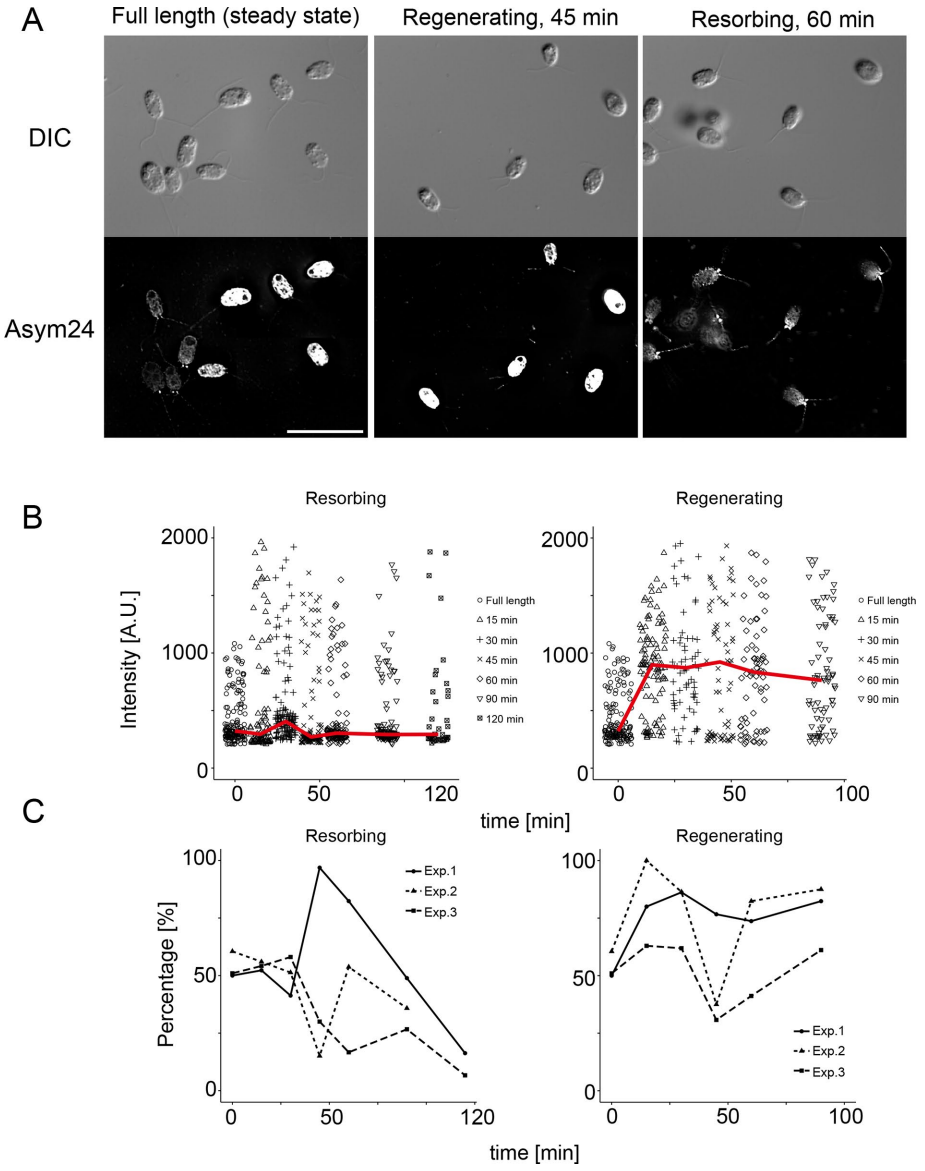

FIGURE 9: aDMA modifications in the cell body of *Chlamydomonas*. (A) Immunofluorescence microscopy using Asym24 antibodies in WT cells with full-length, regenerating, and resorbing flagella. In cells with full-length flagella, half of the cells had weaker cell body staining with basal localization of aDMA-modified proteins. In cells with regenerating flagella (45 min regenerating), almost all cells had a relatively strong cell body signal. In cells with resorbing flagella (60 min resorbing), almost all cells had a weaker signal in the cell body and a strong basal signal in the flagella. Scale bar, 20 μm. (B) The intensities from cell bodies using Asym24 antibodies plotted as a function of time after the initiation of flagellar resorption (left) and regeneration (right). Each data point indicates the intensity from each cell body stained with Asym24. The median values of intensities at each time point are shown with red lines. At 0 min, about half of the cells showed an intensity with a relative value <300, and the other half of the cells had larger cellular intensities. In resorbing flagella, the staining intensity of cells increased, but still a proportion of cells showed lower intensity values, and the median values did not show large changes. However, in regenerating flagella, almost all cells showed an increase in staining intensity, which remained high throughout the time course of flagellar regeneration. (C) Percentages of cells with strong cellular intensities from labeling with Asym24 antibodies plotted as a function of time during flagellar resorption (left) and regeneration (right). In cells with resorbing flagella, the percentage of cells with strong cell body signals decreased to almost 0% at 120 min. In regenerating flagella, all cells showed a similar pattern of change. The percentage of cells with stronger cellular intensities first increased at 15–30 min and subsequently decreased at 45 min. Finally, staining intensities increased at the completion of flagellar regeneration.

fibers, the TZ, particularly the *CEP290* component, forms a gate that controls entry to the flagellum (Craige *et al.*, 2010). This region has been proposed to be involved in modification and control of cargo and IFT particles as they move from the cell body through the basal body region and into the flagella. A number of ciliopathies are caused by sorting errors that occur due to a defect in a TZ component (Szymanska and Johnson, 2012). Because aDMA modifications in other cell types are related to cellular signaling events, it is possible that PRMT 1 and 3 play such a role at the flagellar gate. In addition, the localization of PRMT 1 and the presence of proteins with aDMA modifications distal to the TZ also caught our attention. In the primary cilium, a distinctive proximal segment located distal to the TZ is called the inversin compartment (Shiba *et al.*, 2009; Warburton-Pitt *et al.*, 2012), where INVS/inversin, NPHP-2, and NEK8 are localized. Defects in these proteins cause errors in left/right asymmetry and renal abnormalities (Manning *et al.*, 2013; Czarnecki *et al.*, 2015). The function of this segment in cilia, as well as in *Chlamydomonas* flagella, remains to be elucidated.

Dynamics of basal PRMTs in regenerating and resorbing flagella

In regenerating flagella, the intensity of the immunofluorescence signal from basally located PRMT 1 was low at early times in regeneration (15–45 min after induction; Figure 3, D and E, left). Subsequently both the intensity of label and the amount of localization (measured by percentage of total signal per flagellum) increased. The pattern of staining of aDMA-modified proteins at the base during regeneration was also very similar and comparable to that of PRMT 1 dynamics (Figure 8, E and F, left), as was the pattern of PRMT 3 localization at the base during regeneration (Figure 4, D and E, red curves); however, the recovery of PRMT 3 at the flagellar base during regeneration was not as robust (Figure 4, D and E, green curves). Together these results suggest that PRMT 1 and 3 may be responsible for asymmetric dimethylation of proteins at the flagellar base.

In resorbing flagella, the intensities of signal and the percentage change in PRMTs and aDMA modifications were less similar. Both intensities and percentages of PRMT 1 and 3 at the base during resorption showed the lowest values at 45 min of resorption (Figures 3, D and E, left, and 4, D and E, left);

however, aDMA modification showed the greatest intensities at 45 min of resorption (Figure 8E, left). It is not clear whether PRMT 1 and 3 at the base are related to the aDMA modifications at the base that occur during resorption. Alternatively, the difference summarized here between resorbing and regenerating flagella could be due to the method used to induce resorption. In the presence of IBMX, flagella resorb for about 1 h and then reach a new steady state in which the flagella stabilize at 40–50% of their normal length. The changes in PRMT localization and aDMA modification noted at this time may differ from those in resorbing flagella because the IBMX treated flagella are simply readjusting to a new steady-state length after 1 h.

We do not have a clear explanation for the loss and recovery of PRMTs at the flagellar base during changes in flagellar length; however, we can propose several hypotheses. 1) PRMTs accumulated at the base in full-length flagella during steady state interact with IFT particles and are actively transported into flagella in response to a signal to regenerate or resorb. This hypothesis is consistent with data showing that IFT particles and PRMTs interact more strongly in resorbing flagella (Figure 7, B and C). However, immunostaining with Asym24 antibodies showed that proteins at the base are dimethylated, indicating that PRMTs have at least a basal level of activity in full-length flagella. 2) PRMTs at the base may have roles as suppressors of flagellar dynamics. In this hypothesis, enzyme activity required for the processes of resorption or regeneration is suppressed by protein methylation in full-length flagella. When cells are induced to regenerate or resorb flagella, the signals to do so modify PRMTs, inactivating them and relieving the suppression. This hypothesis is consistent with the observation that Asym24 antibodies do not label the flagellar base during flagellar regeneration. 3) It is possible that methylation has a function parallel to that of protein phosphorylation via cross-talk between the two modification pathways (Biggar and Li, 2015). In this case, methylation may inhibit kinases that are related to flagellar resorption or regeneration, and once PRMT activity at the base is removed, protein phosphorylation occurs and regeneration or resorption takes place. In fact, PRMT 1 inhibits phosphorylation of the transcription factor DAF-16 induced by AKT (protein kinase B) in *Caenorhabditis elegans*, and methylation of DAF-16 occurs near the consensus motif for phosphorylation by AKT (Takahashi *et al.*, 2011).

Tip localization

Accumulation of PRMT 1 and 3 and aDMA modification of proteins also occur at the flagellar tip (Figures 1A and 8, A and B), and this is the region where tubulin and other axonemal proteins were incorporated during growth (Johnson and Rosenbaum, 1992), turned over in full-length flagella at steady flagella, and disassembled during resorption (Marshall and Rosenbaum, 2001; Song and Dentler, 2001). This suggests that protein methylation has a role in axoneme assembly and/or disassembly at the tip. We previously used difference gel electrophoresis to show that the cobalamin-independent form of methionine synthase (MetE) is increased in resorbing flagella (Schneider *et al.*, 2008). In addition, structural components of the axoneme become methylated during flagellar disassembly (Werner-Peterson and Sloboda, 2013). Because flagellar disassembly occurs at the tip, these results strongly suggest that protein methylation is related to tip-specific events, such as flagellar assembly/disassembly, cargo loading/unloading on IFT trains, and perhaps even regulation of motor protein activity.

The present data show that the amount of PRMT 1 at the tip is significantly increased during flagellar regeneration (45–60 min; Figure 3D, right). In addition, the amount of aDMA-containing proteins also increases at the tip during regeneration (Figure 8D). These results indicate that PRMT 1 activity and dimethylation of proteins at the tip are part of the process of flagellar regeneration. In comparison, a significant increase in PRMT 3 at the tip was not observed during regeneration (Figure 4D, right) and was not comparable to that of aDMA modification at the tip (Figure 8, E and F, right, red curves). Thus PRMT 1 but not PRMT 3 is most likely responsible for the aDMA modifications that occur at the tip during regeneration. In resorbing flagella, the intensities and percentages of PRMT 1 and 3 at the flagellar tip are slightly decreased at first (until 45 min of resorption; Figures 3, D and E, right, and 4, D and E, right); however, the amount of aDMA modification at the tip is increased and the percentage of flagella with aDMA modifications was constant at almost 100% throughout flagellar resorption (Figure 8F, right, green curve). These results suggest PRMT 1 (and possibly PRMT3) is more related to flagellar regeneration than flagellar resorption, although further data are needed to support this conclusion. It is also possible that methylation of IFT proteins is related to the unloading of IFT cargo, as Bhogaraju *et al.* (2013) reported as supplementary information that the N-terminus of IFT81/74 might be methylated. Methylation of arginine residues at the N-terminus could reduce the affinity of IFT particles for tubulin, promoting cargo unloading.

Protein methylation varies in the cell body

Staining of the cell body by antibodies directed at aDMA residues differed, depending on the status of the cells. For example, label in the cell bodies of cells regenerating their flagella was strong, and all cells in each field were similarly labeled (Figure 9A, middle). In contrast, cells that were resorbing their flagella showed little or no labeling for aDMA residues in the cell bodies; the small amount of labeling was restricted to the base of the flagella (Figure 9A, right). Populations of cells that had steady-state, full-length flagella exhibited both strong and weak labeling in roughly equal proportions (Figure 9A, left). It is possible that dimethylated proteins in the cell body are related to the enhanced gene expression that occurs during flagella regeneration, although we do not have any direct evidence for this. Note that deflagellation induces high levels of synthesis of flagellar proteins (Lefebvre *et al.*, 1978), and protein methylation is known to regulate gene expression (Bedford and Clarke, 2009). In cells with full-length flagella, cells that have stronger anti-aDMA signals might be the ones in the population that have just completed regeneration of their flagella after a round of cell division.

The control of flagellar growth and resorption is obviously a complex process, involving posttranslational modifications and changes in enzyme activities and enzyme localizations. The work reported here adds new information to our understanding of the events that occur during flagellar growth and disassembly. Future models that describe flagellar growth and resorption will not be complete if they do not include a role for protein methylation in flagellar dynamics.

MATERIALS AND METHODS

Cell strains and culture

C. reinhardtii strain CC125 (wild type, mt$^-$) and *fla10-1* (strain CC-1919, mt$^-$) were obtained from the *Chlamydomonas* Resource Center (http://chlamycollection.org/strains/). NPHP4-HA (*NPHP4-HAN*, mt$^-$; Awata *et al.*, 2014) was generously provided by George Witman (University of Massachusetts Medical School, Worcester, MA). *pf18fla3*::KAP-GFP was generously provided by Junmin Pan (Tsinghua University, Beijing, China); the original KAP-GFP strain was created by Mueller *et al.* (2005) and crossed into *pf18* by Pan when

he was a postdoc with William Snell at UT Southwestern Medical Center. All cells were grown in TAP medium (Gorman and Levine, 1965) at 23°C on a cycle of 14 h of light and 10 h of dark. We used 250 ml cultures for immunofluorescence and fractionation and 8 l cultures for immunoprecipitation.

Phylogenetic analysis

C. reinhardtii PRMT sequences were obtained by tblastn analysis at Phytozome v10.3 (http://phytozome.jgi.doe.gov/pz/portal.html) using human and *Arabidopsis* PRMT sequences as the queries. PRMT sequences from sea urchin (*Strongylocentrotus purpuratus*) were obtained from the National Center for Biotechnology Information. Sequences from human, *A. thaliana*, and rice (*Oryza sativa*) were obtained from UniProt (www.uniprot.org/). Multiple alignments were obtained using ClustalW (http://clustalw.ddbj.nig.ac.jp/), and phylogenetic trees were assembled with the neighbor-joining method of Saitou and Nei (1987) using NJ Plot software.

Antibodies

New England Peptide (Gardner, MA) raised antibodies in rabbits against peptides specific for PRMT 1 (^{311}CKPNAKNPRDLDIS), PRMT 10 (^{365}EQSKTPREFRWNIR), and IFT88 (^{699}YMTKLKKAEKAAVPEA). Specific antibodies from the immune sera were affinity purified (Supplemental Figure S2) versus the corresponding immunizing peptides immobilized on Affigel (Bio-Rad, Richmond, CA) per the manufacturer's instructions. Polyclonal PRMT 3 and PRMT 5 antibodies were purchased from Abcam (Cambridge, MA; Ab91430 [PRMT3] and Ab31751 [PRMT5]). See Supplemental Figure S3 for more information on these antibodies and their potential for use in *Chlamydomonas*. Polyclonal anti-IFT139 and -IFT172 antibodies were provided by Dennis Diener and Joel Rosenbaum (Yale University, New Haven, CT). Anti-IFT81 polyclonal antibodies were provided by George Witman. Asym24 polyclonal antibodies were purchased from EMD Millipore, anti-GFP antibodies were purchased from ThermoFisher-Molecular Probes, and anti–acetylated tubulin and anti-HA antibodies were from Sigma-Aldrich (St. Louis, MO). No fluorescence signals were detected when the secondary antibodies were used alone (Supplemental Figure S4), and there was no bleedthrough from either channel when double-label experiments were analyzed.

Flagellar resorption, regeneration, and isolation

Cells with mature, full-length flagella were induced to resorb their flagella by the addition of IBMX (Sigma-Aldrich) to a final concentration of 0.4 mM (Hartfiel and Amrhein, 1976; Lefebvre *et al.*, 1980). Under these conditions, flagella shorten to approximately two-thirds of their original length by 30 min and are half of the original length after 1 h in IBMX. For regeneration studies, flagella were first detached from the cell body by pH shock (Witman *et al.*, 1972), the cell bodies were collected and resuspended in HMDEK (10 mM 4-(2-hydroxyethyl)-1-piperazineethanesulfonic acid, pH 7.4, 5 mM $MgSO_4$, 1 mM dithiothreitol, 0.5 mM ethylene glycol tetraacetic acid, 25 mM potassium acetate), and flagellar regeneration was allowed to proceed at room temperature with illumination and aeration. For biochemical analyses, flagella detached by pH shock were collected by differential centrifugation as previously described (Sloboda and Howard, 2007).

Fractionation of flagella

After isolation, flagella were suspended at 5 mg/ml in 5% sucrose in HMDEK containing 2 mM 4-(2-aminoethyl)-benzenesulfonyl fluoride hydrochloride (Pefabloc SC; Sigma-Aldrich) and a 1:100 dilution of Halt protease inhibitor cocktail (ThermoFisher) and then frozen at –80°C for 20 min to fracture the membranes. The thawed flagella were rocked for 20 min at room temperature to extract the soluble flagellar matrix proteins and then collected at 12,000 × *g* for 10 min at 4°C. The supernatant (the soluble flagellar components, here called the freeze/thaw supernatant) was removed and stored on ice. The pellet was resuspended in HMDEK, 2 mM Pefabloc, 10 mM Mg-ATP, 0.5% NP-40, and Halt protease inhibitor diluted 1:100 and rocked for 30 min to extract the membrane proteins and IFT components that bound to the axoneme in an ATP-dependent manner. The insoluble axonemes were then collected by a final centrifugation at 12,000 × *g* for 10 min. The supernatant is referred to here as the membrane fraction, although it also contains other proteins released by the presence of the ATP.

Immunoprecipitation

Full-length or resorbing (35 min after addition of IBMX) flagella from *pf18fla3*::KAP-GFP cells were isolated and the membrane plus matrix fraction was obtained as described but without the freeze-thaw step. The membrane plus matrix fraction was clarified at 132,000 × *g* for 10 min at 4°C in a 70.1 Ti rotor (Beckman). For immunoprecipitation (IP), PureProteome Protein G Magnetic Beads (Millipore) were used. The beads were first washed three times with TBST (50 mM Tris, pH 7.4, 150 mM NaCl, 0.5 mM EDTA, 0.02% sodium azide, 0.1% Tween-20). The washed beads were then blocked with 1 mg/ml bovine serum albumin in HMDEK for 1 h at room temperature and then washed three times with TBST. For IP, 25 µg of antibody was added to the IP sample, which was then diluted with an equal volume of ice-cold 2× TBST. The mixture was then incubated with 50 µl of prewashed protein G magnetic beads for 1 h at room temperature. The beads were washed four times with TBST and resuspended a final time in 80 µl of TBST, and 20 µl of 5× SDS–PAGE sample buffer was added, followed by heating to 95°C for 3 min. The beads were then removed and the resulting supernatant analyzed by immunoblotting.

SDS–PAGE and immunoblotting

SDS–PAGE was performed according to the buffer formulations of Laemmli (1970). For immunoblots, proteins were transferred to nitrocellulose membrane, and the membrane was blocked with 5% nonfat dry milk in TBST containing 0.02% sodium azide for 1 h at room temperature. Primary antibodies were diluted in blocking buffer as follows: anti-PRMT 1, 1:100; anti-PRMT 10, 1:200; anti-IFT139, 1:2000; anti-IFT172, 1:5000; anti-IFT88, 1:10,000; anti-IFT81, 1:100; and anti-GFP, 1:5000. The blot was then washed three times, 15 min each, in TBST. Anti-rabbit or anti-mouse antibodies conjugated to horseradish peroxidase (ThermoFisher) at 1:10,000 dilution in blocking buffer were then added and incubated for 30 min, followed by three washes with TBST. Chemiluminescence was detected using SuperSignal West Femto Maximum Sensitivity Substrate (ThermoFisher, Waltham, MA) per the manufacturer's protocol.

Immunofluorescence microscopy

C. reinhardtii cells with full-length, regenerating, or resorbing flagella were fixed with 4% formaldehyde (using paraformaldehyde as the starting material) for 10 min at room temperature. The fixed cells were then extracted with 1% Triton X-100 in phosphate-buffered saline (PBS; 137 mM NaCl, 2.7 mM KCl, 10 mM NaH_2PO_4, 1.8 mM K_2HPO_4, pH 7.4) for 30 min at room temperature. Cells were washed with PBS/Tween-20 three times and then incubated with blocking buffer (see IP protocol) for 1 h at room temperature. Cells were exposed to primary antibodies diluted in blocking buffer

overnight at 4°C. The following dilutions were used: anti-PRMT 1, 1:100; anti-PRMT 10, 1:100; anti-PRMT 3, 1:100; anti-PRMT 5, 1:100; anti-IFT172, 1:200; anti-Asym24, 1:100; and anti–acetylated tubulin, 1:10,000. The samples were washed with TBST four times, 5 min each, and incubated with secondary antibodies diluted in 5% milk in TBST for 2 h at room temperature. Secondary antibodies were Alexa Fluor 488–conjugated goat anti-rabbit immunoglobulin G (IgG) or Alexa Fluor 568–conjugated goat anti-mouse IgG (each diluted 1:200 in blocking buffer; both from ThermoFisher-Molecular Probes). Samples were washed with TBST four times, 5 min each, and mounted in Prolong Gold Antifade with 4′,6-diamidino-2-phenylindole (ThermoFisher-Molecular Probes). Samples were observed with an Axioskop 2 mot plus microscope using a 63×/1.4 numerical aperture Plan Apochromatic objective (Zeiss, Thornwood, NY). Images were projected onto the detector of an ORCA-ER camera (Hamamatsu, Bridgewater, NJ) via an Optivar lens set at a magnification of 2×. The microscope and camera were controlled with MetaMorph software (Molecular Devices, Downingtown, PA). When necessary, images were deconvolved using the AutoQuant software package in MetaMorph and cropped with Photoshop CS5, and figures were composed using Illustrator CS5 (Adobe, San Jose, CA).

Quantitative analysis of labeling as a function of position along flagella

A 16-bit *Z*-stack of tiff images was obtained and deconvolved and a maximum projection produced. Individual flagella in the resulting images were tracked using the ImageJ line tool (Abramoff *et al.*, 2004), and signal intensity along the flagella was measured and saved as a text file. Signal position along the flagella and signal intensity at each position were analyzed using R (version 3.2.1; www.R-project.org/) with the peaks package (version 0.2; http://CRAN.R-project.org/package=Peaks). For signal position presented in the data as histograms in Figures 1, 3, 4, 6, and 8, the length of each flagellum analyzed was divided into 20 equal bins, and the number or intensity of the signals in each 0.05 unit of relative flagella length was counted and reported. Thus fluorescence signals that were more distal than 0.95 times the relative flagellar length were considered to have a tip localization in this analysis, and signals <0.05 times the relative length were considered to have a basal localization. When measuring very short flagella, however, fluorescence signals that were within 0.5 µm of the cell body were designated as having a basal localization, as it was difficult to generate with confidence 20 equal bins in such short flagella. Furthermore, when quantifying shorter-than-normal flagella (i.e., resorbing or regenerating), this analysis compresses the particle counts into a shorter distance, as for all analyses, each flagellum regardless of length was divided into 20 equal portions. Hence the variations noted when comparing full-length, resorbing, and regenerating flagella are likely greater than indicated by the data as presented.

Statistical analysis

Data were plotted using ggplot2 (Wickham, 2009). For comparison of the percentage data relative to enzyme localization (Figures 3E, 4E, and 6F) and protein methylation (Figure 8F), Fisher's exact test was used, with multiple testing correction performed using Holm's method. For comparison of fluorescence intensity values (Figures 3D, 4D, 6G, and 8E), multiple comparisons were performed using the method of Steel and Dwass. For comparison of the localization of PRMT 1 and 3 in *fla10-1* cells (Figure 6H), the data were compared with the Mann–Whitney *U* test.

ACKNOWLEDGMENTS

We gratefully acknowledge the advice and antibodies provided by Tomohiro Kubo and George Witman (UMass Medical Center) and Dennis Diener and Joel Rosenbaum (Yale University). We were supported in this work by the excellent technical assistance of Rita Werner-Peterson and Munaya Sa-eed. Valuable suggestions on the manuscript were provided by Robert A. Bloodgood (University of Virginia Medical Center). This work was supported by National Science Foundation Award MCB 0950402 (R.D.S.), the Ira Allen Eastman (Class of 1829) Professorship at Dartmouth (R.D.S.), which was established in 1910 through a gift to the College by his widow, Jane Eastman, and by a Postdoctoral Fellowship for Research Abroad from the Japan Society for the Promotion of Science (K.M.).

REFERENCES

Abramoff MD, Magalhaes PJ, Ram SJ (2004). Image processing with Image J. Biophoton Int 11, 36–42.

Afzelius BA (2004). Cilia-related diseases. J Pathol 204, 470–477.

Ahmad A, Dong Y, Cao X (2011). Characterization of the PRMT gene family in rice reveals conservation of arginine methylation. PLoS One 6, e22664.

Awata J, Takada S, Standley C, Lechtreck KF, Bellve KD, Pazour GJ, Fogarty KE, Witman GB (2014). NPHP4 controls ciliary trafficking of membrane proteins and large soluble proteins at the transition zone. J Cell Sci 127, 4714–4727.

Bachand F (2007). Protein arginine methyltransferases: from unicellular eukaryotes to humans. Eukaryot Cell 6, 889–898.

Bedford MT (2007). Arginine methylation at a glance. J Cell Sci 120, 4243–4246.

Bedford MT, Clarke SG (2009). Protein arginine methylation in mammals: who, what, and why. Mol Cell 33, 1–13.

Bhogaraju S, Cajanek L, Fort C, Blisnick T, Weber K, Taschner M, Mizuno N, Lamla S, Bastin P, Nigg EA, Lorentzen E (2013). Molecular basis of tubulin transport within the cilium by IFT74 and IFT81. Science 341, 1009–1012.

Biggar KK, Li SS (2015). Non-histone protein methylation as a regulator of cellular signalling and function. Nat Rev Mol Cell Biol 16, 5–17.

Blifernez O, Wobbe L, Niehaus K, Kruse O (2011). Protein arginine methylation modulates light-harvesting antenna translation in Chlamydomonas reinhardtii. Plant J 65, 119–130.

Cole DG, Diener DR, Himelblau AL, Beech PL, Fuster JC, Rosenbaum JL (1998). Chlamydomonas kinesin-II-dependent intraflagellar transport (IFT): IFT particles contain proteins required for ciliary assembly in Caenorhabditis elegans sensory neurons. J Cell Biol 141, 993–1008.

Craige B, Tsao CC, Diener DR, Hou Y, Lechtreck KF, Rosenbaum JL, Witman GB (2010). CEP290 tethers flagellar transition zone microtubules to the membrane and regulates flagellar protein content. J Cell Biol 190, 927–940.

Czarnecki PG, Gabriel GC, Manning DK, Sergeev M, Lemke K, Klena NT, Liu X, Chen Y, Li Y, San Agustin JT, *et al.* (2015). ANKS6 is the critical activator of NEK8 kinase in embryonic situs determination and organ patterning. Nat Commun 6, 6023.

Deane JA, Cole DG, Seeley ES, Diener DR, Rosenbaum JL (2001). Localization of intraflagellar transport protein IFT52 identifies basal body transitional fibers as the docking site for IFT particles. Curr Biol 11, 1586–1590.

Dentler W (2005). Intraflagellar transport (IFT) during assembly and disassembly of Chlamydomonas flagella. J Cell Biol 170, 649–659.

Eitzinger N, Wagner V, Weisheit W, Geimer S, Boness D, Kreimer G, Mittag M (2015). Proteomic analysis of a fraction with intact eyespots of Chlamydomonas reinhardtii and assignment of protein methylation. Front Plant Sci 6, 1085.

Friesen WJ, Paushkin S, Wyce A, Massenet S, Pesiridis GS, Van Duyne G, Rappsilber J, Mann M, Dreyfuss G (2001). The methylosome, a 20S complex containing JBP1 and pICln, produces dimethylarginine-modified Sm proteins. Mol Cell Biol 21, 8289–8300.

Gorman DS, Levine RP (1965). Cytochrome f and plastocyanin: their sequence in the photosynthetic electron transport chain of Chlamydomonas reinhardi. Proc Natl Acad Sci USA 54, 1665–1669.

Hartfiel G, Amrhein N (1976). The action of methylxanthines on motility and growth of Chlamydomonas reinhardtii and other flagellated algae. Is cyclic AMP involved? Biochem Physiol Pflanzen 169, 531–556.
Herrmann F, Fackelmayer FO (2009). Nucleo-cytoplasmic shuttling of protein arginine methyltransferase 1 (PRMT1) requires enzymatic activity. Genes Cells 14, 309–317.
Hu Z, Liang Y, He W, Pan J (2015). Cilia disassembly with two distinct phases of regulation. Cell Rep 10, 1803–1810.
Jahan S, Davie JR (2015). Protein arginine methyltransferases (PRMTs): role in chromatin organization. Adv Biol Regul 57, 173–184.
Johnson KA, Rosenbaum JL (1992). Polarity of flagellar assembly in Chlamydomonas. J Cell Biol 119, 1605–1611.
Kim S, Lee K, Choi JH, Ringstad N, Dynlacht BD (2015). Nek2 activation of Kif24 ensures cilium disassembly during the cell cycle. Nat Commun 6, 8087.
Kozminski KG, Johnson KA, Forscher P, Rosenbaum JL (1993). A motility in the eukaryotic flagellum unrelated to flagellar beating. Proc Natl Acad Sci USA 90, 5519–5523.
Laemmli UK (1970). Cleavage of structural proteins during the assembly of the head of bacteriophage T4. Nature 227, 680–685.
Lechtreck KF (2015). IFT-cargo interactions and protein transport in cilia. Trends Biochem Sci 40, 765–778.
Lee L (2011). Mechanisms of mammalian ciliary motility: insights from primary ciliary dyskinesia genetics. Gene 473, 57–66.
Lefebvre PA, Nordstrom SA, Moulder JE, Rosenbaum JL (1978). Flagellar elongation and shortening in Chlamydomonas: IV. Effects of flagellar detachment, regeneration, and resorption on the induction of flagellar protein synthesis. J Cell Biol 78, 8–27.
Lefebvre PA, Silflow CD, Wieben ED, Rosenbaum JL (1980). Increased levels of mRNAs for tubulin and other flagellar proteins after amputation or shortening of Chlamydomonas flagella. Cell 20, 469–477.
Liang Y, Meng D, Zhu B, Pan J (2016). Mechanism of ciliary disassembly. Cell Mol Life Sci 73, 1787–1802.
Lux FG 3rd, Dutcher SK (1991). Genetic interactions at the FLA10 locus: suppressors and synthetic phenotypes that affect the cell cycle and flagellar function in Chlamydomonas reinhardtii. Genetics 128, 549–561.
Manning DK, Sergeev M, van Heesbeen RG, Wong MD, Oh JH, Liu Y, Henkelman RM, Drummond I, Shah JV, Beier DR (2013). Loss of the ciliary kinase Nek8 causes left-right asymmetry defects. J Am Soc Nephrol 24, 100–112.
Marshall WF, Rosenbaum JL (2001). Intraflagellar transport balances continuous turnover of outer doublet microtubules: implications for flagellar length control. J Cell Biol 155, 405–414.
McBride AE, Silver PA (2001). State of the arg: protein methylation at arginine comes of age. Cell 106, 5–8.
Merchant SS, Prochnik SE, Vallon O, Harris EH, Karpowicz SJ, Witman GB, Terry A, Salamov A, Fritz-Laylin LK, Maréchal-Drouard L, *et al.* (2007). The Chlamydomonas genome reveals the evolution of key animal and plant functions. Science 318, 245–250.
Mueller J, Perrone CA, Bower R, Cole DG, Porter ME (2005). The FLA3 KAP subunit is required for localization of kinesin-2 to the site of flagellar assembly and processive anterograde intraflagellar transport. Mol Biol Cell 16, 1341–1354.
Nakamura S, Takino H, Kojima MK (1987). Effect of lithium on flagellar length in Chlamydomonas reinhardtii. Cell Struct Funct 12, 360–374.
Niu L, Lu F, Pei Y, Liu C, Cao X (2007). Regulation of flowering time by the protein arginine methyltransferase AtPRMT10. EMBO Rep 8, 1190–1195.
Pan J, Naumann-Busch B, Wang L, Specht M, Scholz M, Trompelt K, Hippler M (2011). Protein phosphorylation is a key event of flagellar disassembly revealed by analysis of flagellar phosphoproteins during flagellar shortening in Chlamydomonas. J Proteome Res 10, 3830–3839.
Pan J, Wang Q, Snell WJ (2004). An aurora kinase is essential for flagellar disassembly in Chlamydomonas. Dev Cell 6, 445–451.
Pazour GJ, Agrin N, Leszyk J, Witman GB (2005). Proteomic analysis of a eukaryotic cilium. J Cell Biol 170, 103–113.
Pazour GJ, Dickert BL, Witman GB (1999). The DHC1b (DHC2) isoform of cytoplasmic dynein is required for flagellar assembly. J Cell Biol 144, 473–481.
Piao T, Luo M, Wang L, Guo Y, Li D, Li P, Snell WJ, Pan J (2009). A microtubule depolymerizing kinesin functions during both flagellar disassembly and flagellar assembly in Chlamydomonas. Proc Natl Acad Sci USA 106, 4713–4718.
Piperno G, Mead K (1997). Transport of a novel complex in the cytoplasmic matrix of Chlamydomonas flagella. Proc Natl Acad Sci USA 94, 4457–4462.
Plotnikova OV, Nikonova AS, Loskutov YV, Kozyulina PY, Pugacheva EN, Golemis EA (2012). Calmodulin activation of Aurora-A kinase (AURKA) is required during ciliary disassembly and in mitosis. Mol Biol Cell 23, 2658–2670.
Porter ME, Bower R, Knott JA, Byrd P, Dentler W (1999). Cytoplasmic dynein heavy chain 1b is required for flagellar assembly in Chlamydomonas. Mol Biol Cell 10, 693–712.
Pugacheva EN, Jablonski SA, Hartman TR, Henske EP, Golemis EA (2007). HEF1-dependent Aurora A activation induces disassembly of the primary cilium. Cell 129, 1351–1363.
Quarmby LM, Parker JD (2005). Cilia and the cell cycle? J Cell Biol 169, 707–710.
Saitou N, Nei M (1987). The neighbor-joining method: a new method for reconstructing phylogenetic trees. Mol Biol Evol 4, 406–425.
Schneider MJ, Ulland M, Sloboda RD (2008). A protein methylation pathway in Chlamydomonas flagella is active during flagellar resorption. Mol Biol Cell 19, 4319–4327.
Shiba D, Yamaoka Y, Hagiwara H, Takamatsu T, Hamada H, Yokoyama T (2009). Localization of Inv in a distinctive intraciliary compartment requires the C-terminal ninein-homolog-containing region. J Cell Sci 122, 44–54.
Sloboda RD, Howard L (2007). Localization of EB1, IFT polypeptides, and kinesin-2 in Chlamydomonas flagellar axonemes via immunogold scanning electron microscopy. Cell Motil Cytoskeleton 64, 446–460.
Sloboda RD, Howard L (2009). Protein methylation in full length Chlamydomonas flagella. Cell Motil Cytoskeleton 66, 650–660.
Smith EF, Yang P (2004). The radial spokes and central apparatus: mechanochemical transducers that regulate flagellar motility. Cell Motil Cytoskeleton 57, 8–17.
Song L, Dentler WL (2001). Flagellar protein dynamics in Chlamydomonas. J Biol Chem 276, 29754–29763.
Summers KE, Gibbons IR (1971). Adenosine triphosphate-induced sliding of tubules in trypsin-treated flagella of sea-urchin sperm. Proc Natl Acad Sci USA 68, 3092–3096.
Szymanska K, Johnson CA (2012). The transition zone: an essential functional compartment of cilia. Cilia 1, 10.
Takahashi Y, Daitoku H, Hirota K, Tamiya H, Yokoyama A, Kako K, Nagashima Y, Nakamura A, Shimada T, Watanabe S, *et al.* (2011). Asymmetric arginine dimethylation determines life span in C. elegans by regulating forkhead transcription factor DAF-16. Cell Metab 13, 505–516.
Tobin JL, Beales PL (2009). The nonmotile ciliopathies. Genet Med 11, 386–402.
Warburton-Pitt SR, Jauregui AR, Li C, Wang J, Leroux MR, Barr MM (2012). Ciliogenesis in Caenorhabditis elegans requires genetic interactions between ciliary middle segment localized NPHP-2 (inversin) and transition zone-associated proteins. J Cell Sci 125, 2592–2603.
Wei H, Mundade R, Lange KC, Lu T (2014). Protein arginine methylation of non-histone proteins and its role in diseases. Cell Cycle 13, 32–41.
Werner-Peterson R, Sloboda RD (2013). Methylation of structural components of the axoneme occurs during flagellar disassembly. Biochemistry 52, 8501–8509.
Wickham H (2009). ggplot2: Elegant Graphics for Data Analysis, New York: Springer-Verlag.
Wilson NF, Lefebvre PA (2004). Regulation of flagellar assembly by glycogen synthase kinase 3 in Chlamydomonas reinhardtii. Eukaryot Cell 3, 1307–1319.
Witman GB, Carlson K, Berliner J, Rosenbaum JL (1972). Chlamydomonas flagella. I. Isolation and electrophoretic analysis of microtubules, matrix, membranes, and mastigonemes. J Cell Biol 54, 507–539.
Wloga D, Camba A, Rogowski K, Manning G, Jerka-Dziadosz M, Gaertig J (2006). Members of the NIMA-related kinase family promote disassembly of cilia by multiple mechanisms. Mol Biol Cell 17, 2799–2810.